ABSTRACT

Title of Thesis:	A WAVE CHAOTIC STUDY OF QUANTUM GRAPHS WITH MICROWAVE NETWORKS
	Ziyuan Fu, Master of Science, 2017
Thesis Directed By:	Professor Steven M. Anlage, Department of Electrical and Computer Engineering

Quantum graphs provide a setting to test the hypothesis that all ray-chaotic systems show universal wave chaotic properties. I study the quantum graphs with a wave chaotic approach. Here, an experimental setup consisting of a microwave coaxial cable network is used to simulate quantum graphs. Some basic features and the distributions of impedance statistics are analyzed from experimental data on an ensemble of tetrahedral networks. The random coupling model (RCM) is applied in an attempt to uncover the universal statistical properties of the system. Deviations from RCM predictions have been observed in that the statistics of diagonal and off-diagonal impedance elements are different. Waves trapped due to multiple reflections on bonds between nodes in the graph most likely cause the deviations from universal behavior in the finite-size realization of a quantum graph. In addition, I have done some investigations on the Random Coupling Model, which are useful for further research.

A WAVE CHAOTIC STUDY OF QUANTUM GRAPHS WITH MICROWAVE
NETWORKS

by

Ziyuan Fu

Thesis submitted to the Faculty of the Graduate School of the
University of Maryland, College Park, in partial fulfillment
of the requirements for the degree of
Master of Science
2017

Advisory Committee:
Professor Steven M. Anlage, Chair
Professor Thomas M. Antonsen
Professor Phillip Sprangle

Dedicated to my parents

Fusun Fu

And

Yun Ding

Acknowledgements

I would first like to thank my advisor Prof. Anlage. During my M.S. study at UMD in the past two years, Prof. Anlage is the strongest support for my study and research. He is very kind and patient to all the students and he always gives me a lot of good suggestions for my research. He knows how to guide me to the right approach but not just directly gives me the answer, which truly improves my research ability. At the same time, I want to appreciate the guidance and assistance from my co-advisors, Prof. Antonsen and Prof. Ott. They are both the greatest scientists in the field and they always give me the most value advice for my experiment from the theoretical part. As the committee member, Prof. Sprangle has given me a lot of good comments on my thesis and the presentations for the examination. I really appreciate that.

In addition, I also want to thank my colleagues in this big research group, Bo Xiao, Daimeng Zhang, Seokjin Bae, Bakhrom Oripov, Melissa Trepanier, Min Zhou, Shukai Ma, Trystan Koch, Ke Ma, Adan, Bisrat Addissie and all the persons I have met in the discussions of the group. They all give me great help on research and daily life. Besides, I want to thank for the assistance from the staffs in the departments of physics and ECE, Mary Sutton, Melanie Prange, Bill Churma and Maria Hoo. At last, I want to appreciate the friends I have met in Maryland.

Table of Contents

List of Tables

List of Figures

List of Abbreviations

$\underline{\underline{1}}$ identity matrix

α loss parameter

Δ normalized eigen-energy spacing

A   area

V   volume

τ decay time

λ wavelength

c   speed of light

E   energy

L   length of networks

f   frequency

$\underline{\underline{Z}}$ impedance matrix

$\underline{\underline{Z_0}}$ characteristic impedance matrix

$\underline{\underline{Z_{rad}}}$ radiation impedance matrix

$\underline{\underline{Z_{rad}}}$ ensemble-averaged impedance matrix

EMC   electromagnetic compatibility

EMI   electromagnetic interference

GOE   Gaussian orthogonal ensemble

GUE   Gaussian unitary ensemble

INNS   integrated nearest neighboring spacing

PWB   power balance method

PDF   probability density function

RCM   random coupling model

RMT   random matrix theory

VNA   vector network analyzer

Chapter 1: Introduction

1.1 Motivations

Our daily life is involving more and more electronic devices and technologies. Every day, we are using smart phones, laptops with Wi-Fi, cellular or wireless networks. The electronic devices are all in a very complicated electromagnetic environment. This new trend in real life leads us to think about the problems and mechanisms of electromagnetic coupling and wave propagations in different kinds of systems or environment. This will affect the quality of the usage for the electronics devices or some time may affect the health of our bodies. For researchers in this electromagnetic compatibility and interference (EMC/EMI) field, it is quite interesting to develop efficient electromagnetic interaction models to analyze and understand complicated electromagnetic systems, especially for higher frequencies where the system is very sensitive to small changes.

In real life, more and more complex scenarios in electronics and wave propagation in cavities or through multiple paths make it very difficult to set up precise models [1]. When analyzing a practical electromagnetic problem, we always meet with the challenge that waves propagate in a complicated environment with many details which need to be considered. For example, if we want to analyze the electromagnetic coupling or interference into a complicated system, like a plane, a ship or a building, the structure, the connections between enclosures and the specific details in the system will affect the electromagnetic wave propagating in between these systems.

One may try to find the exact equations and get the exact solutions of wave propagation in the problem. However, it is very hard or even impossible to find such solutions and the exact approach and solutions are changed if just small details in the system are different, and

this is very common in real life. Therefore, it is more practical to solve the problem with a statistical approach. The Random Matrix Theory (RMT) has been applied successfully to describe the wave properties and set up a statistical model of complex systems. The goal for my research is mainly to extend the basic Random Coupling Model (RCM) to analyze the electromagnetic problems in complicated inter-connected systems. So, in this thesis, I mainly study the wave propagation problems based on the Random Coupling Model (RCM) on quantum graphs simulated by microwave networks, which is a simpler model compared to a real complicated system scenarios. This is the basic first-step study that can lead us to solve a more complicated one.

One method to analyze the electromagnetic coupling problem in complex systems is to simplify the system into networks which are the nodes connected by bonds. Then we apply some models or equations to solve for the wave propagation on the networks. For my research, the theory and model are from the Random Coupling Model and I first try to apply those to Quantum Graphs. Quantum graphs are networks with Schrodinger operators on bonds, which are very interesting one-dimensional potentially chaotic systems we can analyze in a wave chaotic approach. Experimentally, we can realize the quantum graphs with microwave networks, which are easy to be set up in the lab just with different junctions and coaxial cables. For the most part of this thesis, I focus on the experimental study of the microwave networks with a simple tetrahedral topology.

1.2 Quantum Graphs

A graph or network is a set of elements which are connected in a certain topology and has applications in many different branches of engineering, science, sociology and biology [2]. A quantum graph, introduced by Pauling in the 1930s, is a linear network structure of vertices connected by bonds with a differential or pseudo-differential operator acting on functions

defined on the bonds [3]. In physics, quantum graphs have been used to model many phenomena, such as acoustic and electromagnetic waveguide networks, quantum Hall systems and mesoscopic quantum systems [2].

Quantum graphs are good models for wave chaos applications from spectral statistics to chaotic scattering and wave function statistics. Methods from quantum chaos and random matrix theory on universality in the spectral fluctuations of quantum graphs have been discussed recently [2]. Researchers have studied quantum graphs experimentally and numerically [4-7]. Quantum graphs have been realized as microwave networks with different topologies such as tetrahedral, irregular hexagon fully connected networks, and fully connected five vertex networks [4-7]. Spectral statistics of graph systems [4,6], the statistics of the reaction matrix K [5,6] and the reflection statistics for one-port graphs [5,6] have been studied, and results from both numerical calculation and experimental measurement show good agreement with theory.
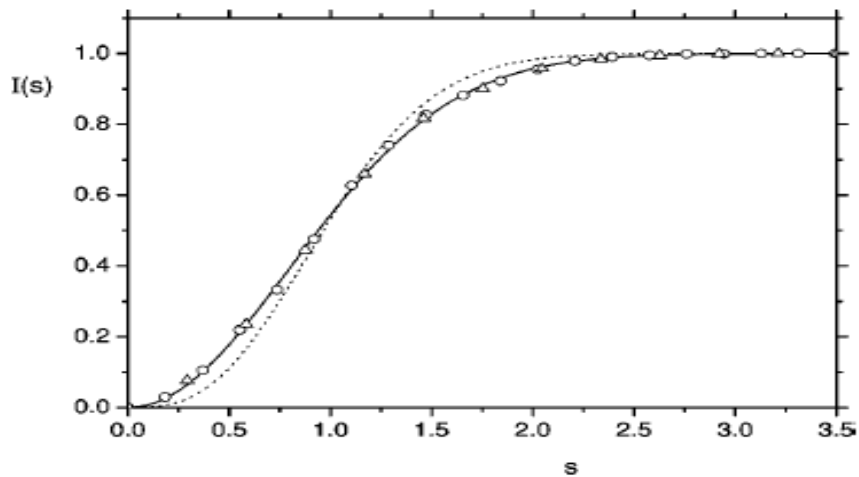
Figure 1.1: Integrated Nearest-neighbor spacing (INNS) distributions from numerical calculations (triangle) and experimental data (circle). Results are compared with theoretical predictions for GOE (solid line) and GUE (dashed line). Reproduced from Ref. [3].

I have listed two examples here from researchers in other groups. The first one is shown

for the integrated nearest-neighbor spacing (INNS) distribution in Fig. 1.1. The solid line is

the theoretical prediction for the GOE case and dashed line is the theoretical predictions for

the GUE case. The GOE and GUE are statistical ensembles of random matrices and are

introduced in section 1.3 Wave Chaos, readers can refer to that part to understand the

definitions and physical meanings of them. Numerical calculations and experimental

measurements were carried out for a 1-port tetrahedral microwave network. The two results

are presented to compare with the theoretical predictions. The triangles show the numerical

calculations and the circles show the experimental data. We can see both results agree with

the GOE predictions well, which are from graphs or networks with time reversal invariance.
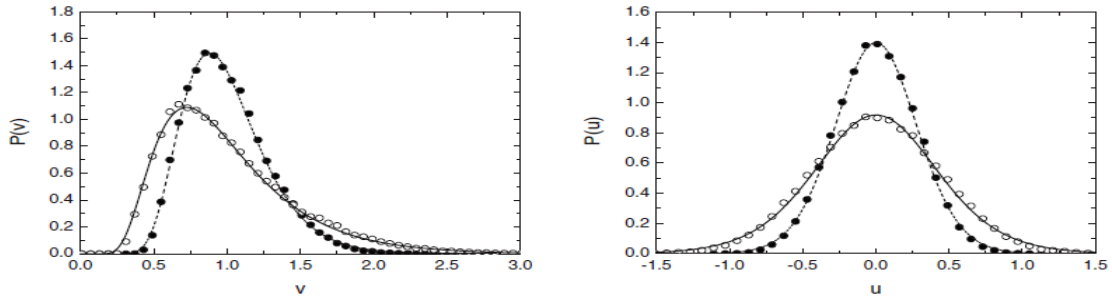
Figure 1.2: Numerically calculated distribution of the imaginary part (v) and the real part (u) of the K matrix compared with the theoretical predictions. Reproduced from Ref. [5].

Another example shows the impedance statistics of the quantum graphs. In Fig. 1.2,

probability density functions (PDF) of impedance statistics from numerical calculations are

fit to the predictions from analytical calculations of the K matrix. Both the real part and

imaginary part of the impedance statistics agree well with theoretical predictions with

different loss in the quantum graph, as shown in solid dots and empty dots. The INNS and the

PDFs of the impedance statistics both show that the quantum graphs have similar statistical behavior as expected for quantum chaos systems. However, in the following chapters, from the experiments we have done, we find out that one cannot directly apply these theories to describe the features of finite-sized quantum graphs.

Let us analyze the wave propagations on the bonds of the quantum graph. We can endow the graphs with a metric which will enable us to define the Schrodinger operator on the graph. The Schrodinger operator of the one-dimensional operators associated with each bond is [2]:

$$H_b = \left[(\frac{1}{i} \frac{d}{dx_b} + A_b)^2 + w_b(x_b) \right],$$ (1.1)

where $w_b(x_b)$ is a non-negative potential function and smooth on the bond. A_b are real, positive constants and represent the vector potential.

In spectral theory, the trace formula is a useful tool. The trace formula represents a sum over periodic orbits of the underlying classical dynamics.

The state counting function can be expressed by a smooth term (the Weyl term) and an oscillating term

$$N(k) = N_{Weyl}(k) + N_{osc}(k),$$ (1.2)

and the Weyl term is given as

$$N_{Weyl}(k) = \frac{BL}{\pi} k + N_{Weyl}(0),$$ (1.3)

From the first term $\frac{BL}{\pi} k$, we can see in the quantum graphs, the counting function is linearly increasing with wavenumber or frequency. That is different from the two-dimensional or three-dimensional systems. For the quasi-two-dimensional system, the mean-spacing between the eigenvalues $\Delta k_n^2 \cong 4\pi/A$, where A is the area of the system. And for the three-dimensional system $\Delta k_n^2 \cong 2\pi^2/(kV)$, where V is the volume of the system.

1.3 Wave Chaos

We are interested in the solutions of wave equations when the quantum mechanical wavelength is much shorter compared with the size of the system to be analyzed. The statistical models we use in this thesis are based on the theory from nuclear physics and quantum wave systems [8,9]. Because the density of energy levels is high, especially at high energy, and solution of the wave equations was not possible, so Wigner proposed the statistical approach about the problem. The statistical approach to wave equations in physics is called 'quantum chaos' [8, 9]. Wigner used a random matrix from a certain ensemble to replace the Hamiltonian matrix $\underline{\underline{H}}$. Their analysis showed that the statistical properties of the eigenvalues of the random matrices agree with those of real nuclei. This approach is the well-known 'random matrix theory'. Eugene Wigner [10] studied the energy levels of large nuclei.

Consider the n×n random Hamiltonian matrices and compute the eigenvalues k^2. Δk_n^2 is the mean spacing of the eigen-energy. Weyl [11] showed results for the approximate average eigenvalue density for the much smaller wavelength compared to the size of the system. We can normalize the spacing using the Weyl formula,

$$s_n = \frac{(k_{n+1}^2 - k_n^2)}{\Delta k_n^2},\qquad (1.4)$$

Depending on the symmetries, there are two cases mostly considered, which are the Gaussian Orthogonal Ensemble (GOE) and Gaussian Unitary Ensemble (GUE). The results for the nearest-neighbor spacing probability distributions are [10];

For GOE case,

$$P_{GOE}(s) \cong \left(\frac{\pi}{2}\right) s \, exp\left(-\frac{\pi s^2}{4}\right),\qquad (1.5)$$

and for GUE case,

$$P_{GUE}(s) \cong \left(\frac{32}{\pi}\right) s^2 exp\left(-\frac{4s^2}{\pi}\right),\qquad (1.6)$$

The GOE ensemble is invariant under orthogonal conjugation, and it models Hamiltonians with time-reversal symmetry. The GUE ensemble is invariant under unitary conjugation and it models Hamiltonians lacking time-reversal symmetry. In this thesis, we will examine both of the cases in experiment.

The basis for most of the previous work on statistical electromagnetics is the random plane wave hypothesis. With some assumptions, the fields in the cavity behave as a random superposition of isotropically propagating plane waves. The predictions from the random plane wave hypothesis are consistent with eigenfunction statistical data in the cases of time reversal symmetry and of broken time reversal symmetry [12]. As the wavelength becomes much smaller compared to the size of the cavity, scarring becomes less and less significant, occurring on a smaller and smaller fraction of modes and with smaller energy density enhancement near the associated periodic orbit [13].

1.4 Complicated Systems with Electromagnetic Topology Analysis

As mentioned in the Motivations, one of the goals for this thesis is to analyze the electromagnetic problem for complicated wave systems. And one approach to deal with the problem is to replace the complicated systems with networks which are formed by nodes connected by bonds.

From my knowledge of some previous traditional papers and notes, I will summarize some key points in the electromagnetic topological analysis. The goal of this method is to understand how electromagnetic energy penetrates a complex enclosure and propagates into each sub-enclosure. An example is shown in Fig. 1.3. The Power Balance Method is used to analyze energy propagation in this case. In this method, we shall assume that all the volumes or cavities are perfectly shielding with walls, and the wave can only couple into the cavities through apertures on the walls or cables.

7

a) Computation of the Power Density in the test area

$\vec{E}_{inc}$

b) Computation of the mean power density in cavities
=F(Quality factors, coupling cross sections of POE, internal topology)

$\vec{H}_{inc}$ $\vec{k}_{inc}$

O7 O8 O9

C3

O4 O5

O1 O3 C2

C1 O2

c) Computation of the Power induced on cables at equipment input

O6

C4

d) Computation of mean power density in equipment

(a)

V_0

$V_{1,1}$
(C3)

$V_{2,6}$ $V_{2,4}$
(B2)

$V_{3,1(B4)}$

$V_{2,1}$ $V_{3,3}$
(C4)

$V_{2,2}$ $V_{2,5}$ $V_{2,7}$ $V_{2,3}$
(B1) (B3)

$V_{3,2(B5)}$

$V_{1,2}$
(C1)

$V_{1,3}$
(C2)

O7 - O8 - O9

C3

O4 O5

C1 O3 B2

O1 C2 O6

B4 C4

B1 O2 B3 B5

V_0

O1 O7-O8-O9

O4 $V_{1,1}$ O5

$V_{1,2}$ O3-O2 $V_{1,3}$

O3 $V_{2,6}$ $V_{2,4}$ O6

$V_{2,2}$ $V_{2,5}$ O2 $V_{2,1}$

$V_{2,7}$ $V_{2,3}$

$V_{3,1}$ $V_{3,3}$ $V_{3,2}$

(b)

Figure 1.3: Example of application of the PWB method to topologically decompose a real system into shielding diagram and interaction sequence diagram [14]. In (a), a real

system is simplified into equipment level with the volumes, coupling cross sections, running cables and so on. In (b), the mean dissipated power and mean power density are associated to the nodes. Branches between nodes represent the propagation of the power. Reproduced from Ref. [14].

In Fig. 1.3, I have shown an example for how to decompose a real problem with the effects of electromagnetic coupling into a network representation. With EM topology-based approach [36], the system can be replaced with an interaction sequence diagram, which follows the running of the power transferred into the cavities. In the Power Balance Method (PWB) [14], the model is like a plumbing model for energy flow. All of the connections in the diagram are considered to be of zero length. In other words, interference effects and delay phase shifts are completely ignored in this treatment. Compared to the more sophisticated treatment we want to include interference effects, this example gives us some useful hints. When analyzing a complicated system with the RCM, we can apply a similar way to decompose the system into equipment level and form a network. The difference will be that in the RCM, we need to consider the interactions and model the interactions between bonds and nodes. In other words, we want to retain the interference effects for wave propagation between nodes. We can numerically calculate the statistical power transfer in the RCM and compare the accuracy of results with the PWB.

1.5 Outline of the Thesis

In this chapter, I have introduced a big picture of the wave chaotic study related to the thesis. In the following chapters, I will talk about the details of the theory, the experiments and some new investigations related to wave chaos and will focus on the non-universal features of the simple microwave network.

Chapter 2 introduces the Random Coupling Model, which is the main theory we used in the experiments of the thesis. The models are developed by previous members in our group. Basically, for my M.S. study, I mainly capture the model and apply it into my experiment on Microwave Networks.

In Chapter 3, I will introduce some investigations I have done based on the Random Coupling Model, which may be useful in some aspects. The first part is to compare the Random Coupling Model with the Power Balance Method. Equations are derived and statistical results are presented from numerical calculations and experimental data. The second part is the comparison between the Random Coupling Model and a similar K-matrix theory. In that part, I have numerically calculated the impedance statistics in the GUE case. The last part is about the Random Coupling Model impedance statistics with different loss parameters. This will become a strong supporting evidence for the way we deal with the experimental data.

In Chapter 4, I focus on the experimental results of the microwave networks. I will introduce some basic features of the microwave networks including the radiation impedance, and networks with/without time reversal invariance. Next I will talk about the impedance statistics of the networks from experiment and apply the Random Coupling Model to describe the statistical properties. Finally, I will discuss the non-universal features of long-range statistical properties of the networks.

In Chapter 5, I will make conclusions for the thesis and give some suggestions for future work.

Chapter 2: The Random Coupling Model

The random coupling model (RCM) describes the coupling of radiation into and out of electrically large enclosures with chaotic ray dynamics [1]. The RCM gives a prescription for determining both the universal and non-universal features of the experiment. The RCM has successfully analyzed the statistical properties of the impedance (Z) and scattering (S) matrices of open electromagnetic cavities where the waves are coupled through transmission lines or waveguide [15]. In [16, 17], a 2D chaotic $\frac{1}{4}$-bowtie cavity and in [18] a 3D chaotic GigaBox cavity have been studied and impedance statistics have been analyzed from experimental measurement. In this thesis, the RCM is applied for the analysis of electromagnetic propagation in quasi-one-dimensional microwave networks.

2.1 Basic Random Coupling Model

The Random Coupling Model was first introduced by Zheng *et al*.[19]. The random plane wave hypothesis and random matrix theory (RMT) are used to describe the statistical properties of the impedance matrix $\underline{\underline{Z}}$ of a wave chaotic system, and the system-specific features which are incorporated through coupling ports.

In the linear case, a system can be modeled as an N-port network where the wave can scatter in and out through the coupling ports. And for the N-port system, the $N \times N$ cavity impedance matrix can be expressed as

$$\underline{\underline{Z}}_{cav} = jIm\left[\underline{\underline{Z}}_{rad}\right] + Re\left[\underline{\underline{Z}}_{rad}\right]^{1/2} \underline{\underline{z}} \, Re\left[\underline{\underline{Z}}_{rad}\right]^{1/2}, \tag{2.1}$$

In Eq. (2.1), the impedance matrix of the cavity is obtained by the universal fluctuating property predicted by RMT $\left(\underline{\underline{z}}\right)$ and the system-specific features $\left(\underline{\underline{Z}}_{rad}\right)$.

The matrix $\underline{\underline{z}}$ in Eq. (2.1) is the normalized impedance, the statistical properties of which can be predicted by random matrix theory, and the $\underline{\underline{z}}$ matrix describes the universal fluctuation properties.

In [1], the normalized impedance $\underline{\underline{z}}$ can be modelled as,

$$\underline{\underline{z}}(k_0) = -\frac{i}{\pi} \sum_n \frac{\phi_n\, \phi_n^T}{\frac{k_0^2 - k_n^2}{\Delta k^2} + i\alpha}, \tag{2.2}$$

where $\underline{\phi_n}$ is a vector of length M for an M-port system. The elements of $\underline{\phi_n}$ are the variables describing the coupling of each mode n to the ports. We assume that the Berry hypothesis applies so that on average the statistical properties of the fields at any point inside the system are described by a random superposition of plane waves of all possible directions and phases. Based on this hypothesis we take the $\underline{\phi_n}$ to be Gaussian random variables, which follows from the random plane-wave hypothesis, and this assumption will be called into question for finite-size graphs later in the paper. Also, Δk^2 is the mean mode spacing of the closed system, which can be approximated by Weyl's formula in the limit of small wavelength compared to the system size.

For two-dimensional systems,

$$\Delta k^2 \cong \frac{4\pi}{A}, \tag{2.3}$$

where A is the area of the enclosure.

For three-dimensional systems,

$$\Delta k^2 \cong \frac{2\pi^2}{kV}, \tag{2.4}$$

where V is the volume of the cavity.

And for the quasi-one-dimensional system which will be investigated in the following chapters,

$$\Delta k^2 \cong \frac{2\pi k}{L\sqrt{\varepsilon}}, \qquad (2.5)$$

where L is the total length of the graph or network and ε is the dielectric constant of the coaxial transmission line.

The k_n are the closed cavity mode wavenumbers and k_0 is the wavenumber of interest. We take the spectrum of eigenmodes k_n to be that of a Gaussian orthogonal random matrix for time-reversal invariant systems. The statistically fluctuating properties of the normalized impedance $\underline{z}$ in the RCM is determined by a single loss parameter α, defined as

$$\alpha = \frac{k_0^2}{\Delta k^2 Q}, \qquad (2.6)$$

where Q is the loaded quality factor of the cavity or network. The losses are assumed uniformly distributed in the graph, and the variation of the Q from one mode to the next is expected to be small, so that an average Q meaningfully quantifies the degree of loss. The loss parameter can also be thought of as the ratio of the 3-dB bandwidth of a typical mode to the mean spacing of the modes. As such, the loss parameter is a slowly varying function of frequency in most systems. A lossless system has $\alpha = 0$, and typical systems encountered in real life have loss parameters between 0.1 and 10.

The loss parameter α can be calculated directly through knowledge of the average quality factor over a certain frequency range, along with knowledge of the length of the graph. This gives an alternate way which can be compared with the loss parameter obtained from fitting PDFs of normalized impedance $\underline{z}$ extracted from experimental data. In Fig. 2.1 we can see that the PDFs of $\underline{z}$ are only dependent on the loss parameter α.
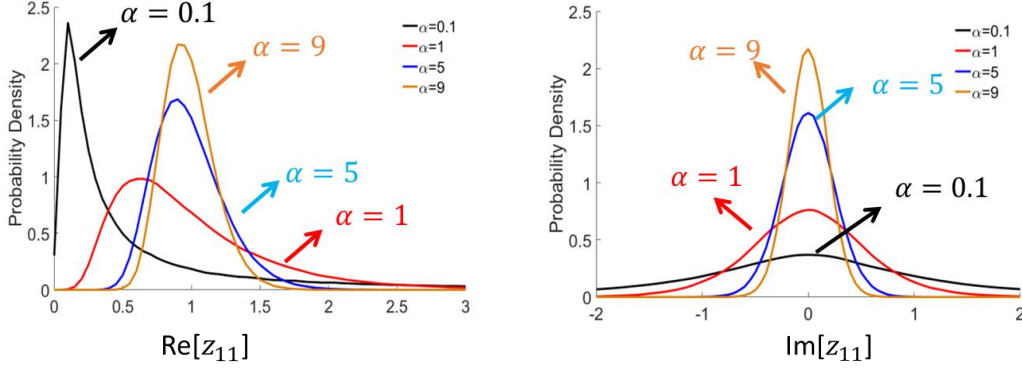
Figure 2.1: Random Matrix Theory predictions for the PDFs of real and imaginary part of normalized impedance with different α for a one-port wave chaotic system with time-reversal invariance symmetry Hemmady *et al*.[34].

2.2 The Random Coupling Model with Short-Orbit Corrections

Hart *et al*. [20] introduced an extended Random Coupling Model which includes the short-orbit effect

$$\underline{\underline{Z}}_{cav} = jIm\left[< \underline{\underline{Z}}_{cav} >\right] + Re[< \underline{\underline{Z}}_{cav} >]^{1/2}\underline{\underline{z}}\,Re[< \underline{\underline{Z}}_{cav} >]^{1/2}, \qquad (2.7)$$

The matrix $< \underline{\underline{Z}}_{cav} >$ is the ensemble-averaged cavity impedance matrix, which captures the system-specific features, including the radiation impedance of the ports and short-orbits that exist in the ensemble [21]. Short orbits are trajectories that go from a port and bounce a limited number of times before the energy leaves the graph through the same port or another port. This should be contrasted with longer orbits, which contribute to the universal impedance fluctuations.

In the real experiments, when measuring the statistics of wave scattering properties, we need an ensemble measurement of the system with many different realizations. We can typically vary the geometrical configurations of the cavities or networks locally or globally. In addition the measurements can be taken at different frequencies.[17,22,23,24,25]. These

variations create different realizations that have the same universal system properties, with a fixed contribution from the system-specific details. This will require that we can create an ensemble of the system with a high statistical quality. In the first tests of the microwave network realization of quantum graphs, we did not get very good realizations from experiments, which prevented application of the RCM with the short orbits effects. In Chapter 3, I will check the quality of the ensemble from the experimental data utilizing a quantitative measure.

Chapter 3: Investigations with the Random Coupling Model

I name this chapter "investigations with the RCM", meaning that there are "little" new things I have found during this thesis study. Section 3.1 shows the results when I was investigating the power balance method and comparing it with the Random Coupling Model. Section 3.2 shows the results of comparisons between theory of the Random Coupling Model and the K matrix. This came about when I was investigating the previous research related with quantum graphs. Section 3.3 discusses the impedance statistics from the RCM with different loss parameters. I have summarized these results when I was getting the PDFs of the normalized impedance statistics from the experimental data.

All these results I put in this chapter, I hope, will give some hints for further study related to the RCM and the EMC/EMI problems.

3.1 Power Balance Method and the Random Coupling Model

A network formulation of the power balanced method was introduced by Jean-Philippe Parmantier and colleagues [14] to estimate high frequency coupling mechanisms in complex systems. The power balanced method (PWB) is based on statistical concepts and some parameters in this method are considered to be not precisely known. The main assumption is that the dimension of the system under test is much larger compared to the wavelength of the electromagnetic wave, which is the same as in the RCM. The power balanced method also incorporates some of the concepts of the RMT. As the RCM and power balance method can solve similar electromagnetic problems and some assumptions are the same, it is very interesting to compare the two models.

Based on the equations in [14] computed with the PWB approach, for the single cavity case, the variance of S_{21}, σ^2_{S21}, which represents the power transfer between two coupling ports, can be derived as:

$$\sigma_{S21}^2 = \frac{\lambda^3 Q}{16\pi^2 V}(1 - |S_{11}|^2)(1 - |S_{22}|^2), \qquad (3.1)$$

where λ is the wavelength, Q is the quality factor and V is the volume of the cavity. S_{11} and S_{22} are the measured S-parameter of the waveguide or antenna attached to the coupling ports. The measured S-parameters are considered to be made up of un-stirred components and stirred components [37]. In the measurements, there are line of sight paths and signals that are transferred between the antennas or waveguides that do not interact with the mode-stirrers. The variance of S_{21}, σ_{S21}^2, removes the unstirred components and represents the mean transferred power.

In this case, the pre-factor on the right hand side of Eq. 3.1 is constant, and the scattering parameter values vary rapidly with frequency. We can use Eq. 3.1 to numerically calculate the variance of S_{21} and predict the mean transferred power between the two ports.

In the RCM, for the 3D cavity case, the loss parameter $\alpha = \frac{k^3 V}{2\pi^2 Q}$, and the wavelength λ is related to the wavenumber k by $\lambda = \frac{2\pi}{k}$. Based on the equations above, the variance of S_{21}, σ_{S21}^2, in the RCM can be derived as,

$$\sigma_{S21}^2 = \frac{1}{4\pi\alpha}(1 - |S_{11}|^2)(1 - |S_{22}|^2), \qquad (3.2)$$

The S_{11} and S_{22} are the reflection coefficients of the antennas or waveguides. In the calculations for Eq. (3.2), I try two ways to get the reflections of the antennas or waveguides used in this experiment. 1) The radiation impedance of the waveguides or antennas. 2) The averaged S parameters over all the realizations. Both of the cases will be discussed below.

To test Eq. (3.2), experimentally measured data in a 3-D Gigbox are used from our collaborators at NRL [18]. The data was taken in frequency ranges from 3.7 GHz to 5.5 GHz and 5.5 GHz to 8.25 GHz.

The variance of S_{21}, σ_{S21}^2, can be calculated from the experimental data as follows [14],

$$\sigma_{s21}^2 = E\left[\left|S_{21}^i\right|^2\right] - \left|E\left[S_{21}^i\right]\right|^2 = \frac{1}{N-1}\sum_{i=1}^{N}\left|S_{21}^i\right|^2 - \frac{N}{N-1}\left|\frac{1}{N}\sum_{i=1}^{N}S_{21}^i\right|^2, \qquad (3.3)$$

where N is the number of realizations in the ensemble, and S_{21}^i are the raw data of different realizations.

To estimate the quantity σ_{s21}^2 in the RCM method, the key parameter is the loss parameter α. The α values should be as precisely known as possible over the frequency range under test. Hence, the data are cut into small frequency ranges and α values are calculated for each of them. In Fig. 3.1 (a), the α values are shown for ten frequency ranges from low to high. We can see that the α value is discontinued around 6 GHz, which I believe may be caused by some materials with a higher loss in the cavity around 6 GHz. The α values are found by fits of the PDFs of normalized impedance from measured data to the RCM predictions. This process is the same as will also be shown in Chapter 4 for the analysis of the impedance statistics of microwave networks. The measured scattering matrix ensemble data for each of the small frequency ranges can be used to examine the statistics of the normalized impedance matrix $\underline{\underline{z}}$ in Eq. (2.7) and compared to the predictions of RMT in Eq. (2.2). In Fig. 3.2(b), we can see that the PDFs of the normalized impedance from experimental measurements agree well with the RCM predictions, which ensures that the loss parameter α we used in the calculations is very accurate.

(a)

18
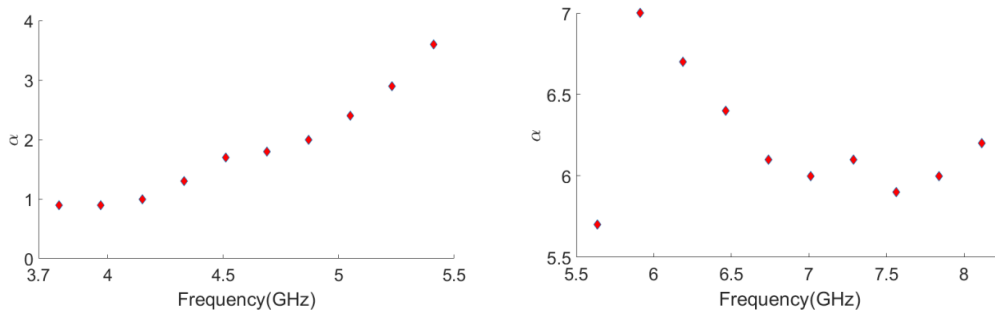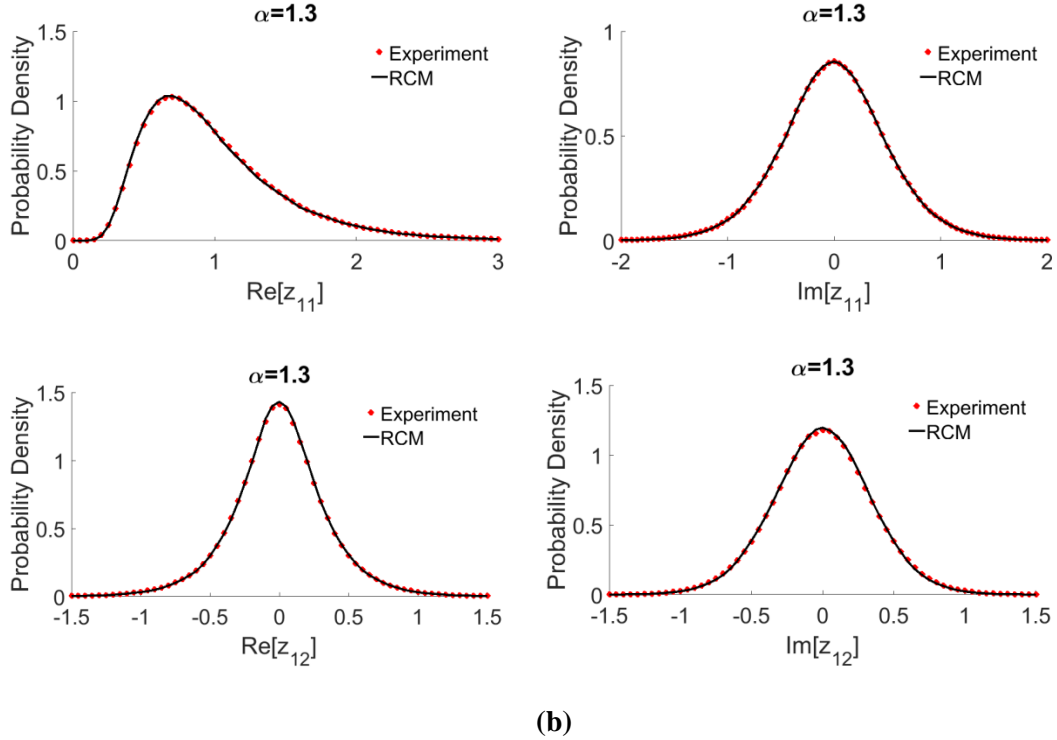
Figure 3.1: (a) α values of the cavity in [18] over the 3.7-5.5 GHz and 5.5-8 GHz ranges. The cavity is a 2-port reverberation chamber (rectangular aluminum box with dimensions of 1.22 m × 1.27 m × 0.65 m). (b) PDFs of normalized impedance (z_{11} and z_{12}) from the experimental measurements (4.3 GHz to 4.5 GHz) fits to the RCM predictions.

After the α values have been obtained, Eq. (3.2) can be used to estimate the variance of S_{21}. First, the radiation impedances of the waveguides or antennas are applied in the computation and the results are shown in Fig 3.2. Because the cavity is a very large one, it is not that easy to measure the radiation impedance if we use the traditional way in which we put absorbers on all the inner walls and measure the radiation impedance. In [35], a time gating technique was introduced to obtain the radiation impedance, which is applied for this cavity.

19
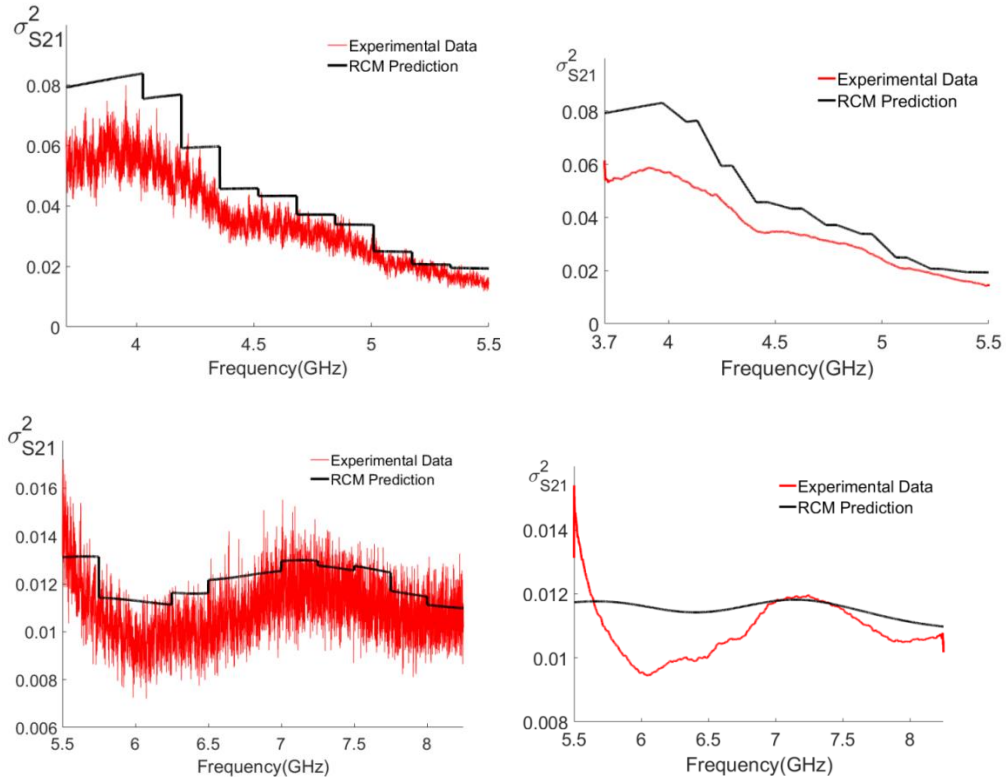
Figure 3.2: Variance of S_{21} of the 3-D Gigbox over the two frequency ranges. Black curves are the RCM computation with radiation impedance and the red curves are the experimental data calculated from Eq. (3.3).

The curves in the right two plots in Fig. 3.2 are the curves in the left two plots smoothed by averaged in a frequency range of 75 MHz. As shown in Fig 3.2, the computation results from RCM method agree well with the experimental data. Next, the averaged S parameters over all the realizations are applied in the computation and the results are shown in Fig. 3.3.
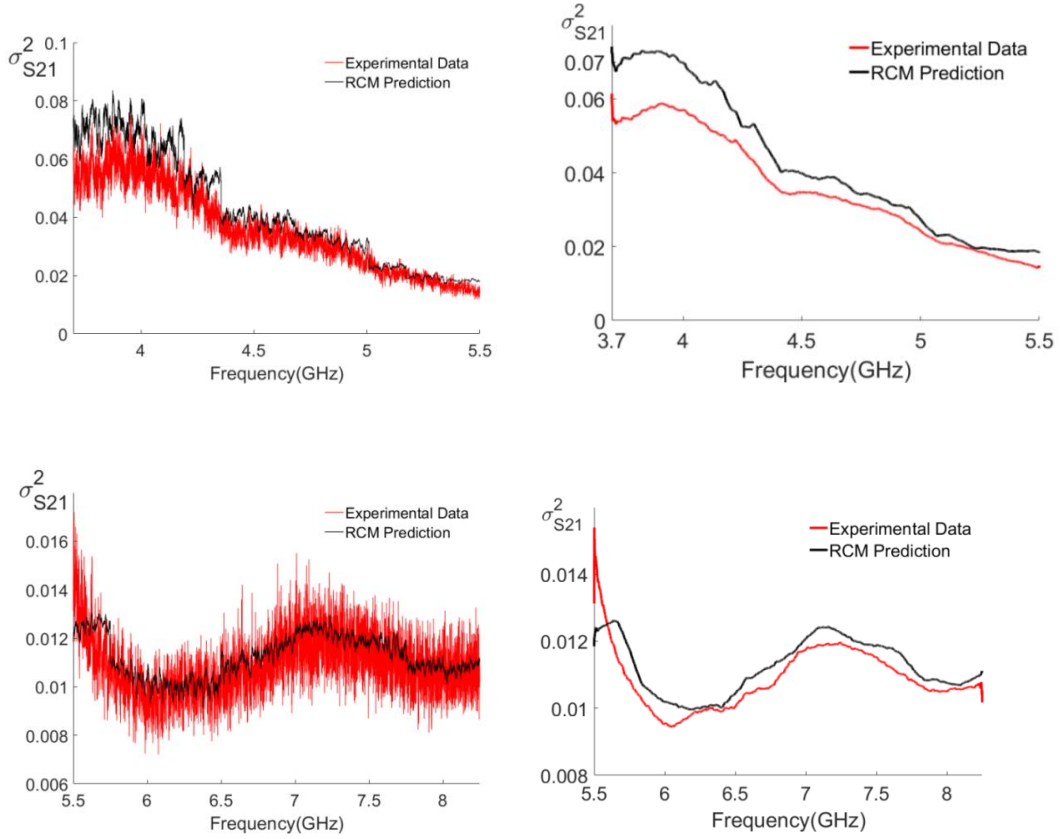
Figure 3.3: Variance of S_{21} of the 3-D Gigbox over the two frequency ranges. Black curves are the RCM computation with averaged S-parameters and the red curves are the experimental data.

Compared to the curves in Fig 3.2, the deviations between the predictions and experimental data are smaller. The reason is that the averaged S parameters incorporate the short-orbits effects in the cavity, which incorporate more specific-details in the system.

In the above, we have numerically calculated the power transfer represented by σ_{S21}^2 using the RCM, for a single cavity case. The results in Fig. 3.2 and Fig. 3.3 show that the calculations predict the experimental data well, which means this numerical calculation method works well for the power transfer in the one cavity case.

Following similar derivations, the computations for σ^2_{S21} of multiple cavities in a certain topology can be obtained. For example, the expression of σ^2_{S21} for two coupled cavities should be,

$$\sigma^2_{S21} = \frac{1}{4\pi\alpha_u\alpha_l}\frac{<\sigma>}{\lambda^2}(1 - |S_{11}|^2)(1 - |S_{22}|^2), \tag{3.4}$$

where the α_l and α_u are the loss parameter in the lower and upper cavities, $<\sigma>$ is the average coupling cross section and λ is the wavelength of interest.

We can test the Eq. (3.4) once we have a high quality data set from measurements of two coupled cavities. And following the theories with different topologies, we can derive the equations with more complicated networks.

3.2 K-Matrix and the Random Coupling Model

In the RCM, the normalized impedance matrix $\underline{\underline{z}}$ describes the universal statistical properties of a chaotic system. Fyodorov and Savin have found the joint distribution function of the local Green function for a chaotic system with a uniform energy loss or absorption, which is known as the K matrix [26]. In this part, the two kinds of impedance matrices will be compared with various losses in both the GOE and GUE cases.

The direct relationship between the K matrix and Z is that $iK \equiv Z$. Thus, the imaginary part v of the K matrix is the real part of $\underline{\underline{z}}$ and the real part u of the K matrix is the imaginary part of $\underline{\underline{z}}$. The explicit form for the distributions of the real part u and imaginary part v of the K matrix at arbitrary absorption are calculated in the GOE and GUE case [26].

In the GOE case,

$$P_u(u) = \frac{\mathcal{N}_1 e^{-\gamma/4}}{2\pi\tilde{u}}\left[\frac{A}{2}\sqrt{\frac{\gamma}{4}}D\left(\frac{\tilde{u}}{2}\right) + BK_1\left(\frac{\gamma\tilde{u}}{4}\right)\right], \tag{3.5}$$

$$P_v(v) = \frac{\mathcal{N}_1 e^{-a}}{\pi\sqrt{2\gamma}v^{\frac{3}{2}}} \left(A[K_0(a) + K_1(a)]a + \sqrt{\pi}Be^{-a}\right), \tag{3.6}$$

and in the GUE case,

$$P_u(u) = \frac{\gamma}{2\pi}\left[sinh\frac{\gamma}{2}K_0\left(\frac{\gamma\tilde{u}}{2}\right) + \frac{cosh\frac{\gamma}{2}}{\tilde{u}}K_1\left(\frac{\gamma\tilde{u}}{2}\right)\right], \tag{3.7}$$

$$P_v(v) = (\gamma/16\pi)^{1/2}v^{-3/2}exp\left[-\frac{\gamma(v + v^{-1})}{4}\right] \times \left[2cosh\frac{\gamma}{2} + (v + v^{-1} - 2/\gamma)sinh\frac{\gamma}{2}\right], \tag{3.8}$$

where $\tilde{u} \equiv \sqrt{u^2 + 1}$ and $a \equiv \frac{\gamma}{16}\left(\sqrt{v} + 1/\sqrt{v}\right)^2$ with α-dependent constants $A \equiv e^\alpha - 1$ and

$B \equiv 1 + \alpha - e^\alpha$. The parameter α is a quantity scaling the absorption parameter as $\alpha \equiv \gamma\beta/2$,

where γ is the dimensionless absorption strength and β is the Dyson index counting the

number of real components per matrix element in the random matrices (i.e. $\beta = 1$ for GOE

and $\beta = 2$ for GUE). $K_v(z)$ is the MacDonald function and

$D(z) \equiv \int_0^\infty dq\sqrt{1 + z(q + q^{-1})}e^{-\gamma z(q+q^{-1})/4}$ is introduced for convenience.

In the equations above, the absorption parameter γ can be related to the loss

parameter α in the RCM as $\gamma = 4\pi\alpha$, which has been shown in Hemmady *et al.*[34].

First, in the GOE case, the PDFs of real and imaginary parts of the K matrix and the $\underline{\underline{z}}$

matrix with different loss parameters are compared below.
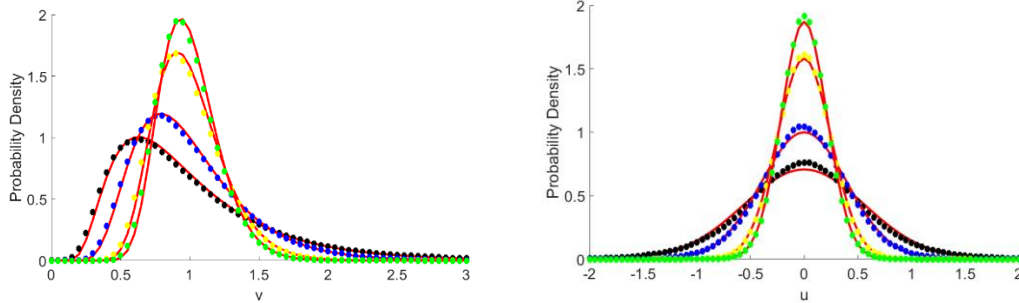
Figure 3.4: PDFs of real and imaginary part of K-matrix from analytical calculations and real and imaginary part of $\underline{\underline{z}}$ matrix from numerical calculations in GOE cases. The five red curves are PDFs of K-matrix from analytical calculations with γ =12.6, 25.1, 62.8, and 88.0. The dots represent the numerical calculations from the RCM, black ($\alpha = 1$), blue ($\alpha = 2$), yellow ($\alpha = 5$), green ($\alpha = 7$).

In Fig. 3.4, PDFs of impedance statistics from the RCM of four loss parameters are shown, that is α = 1 (black dots), α = 2 (blue dots), α = 5 (yellow dots) and α = 7 (green dots). As mentioned above γ = 4πα, so the four red curves are the PDFs of impedance statistics from K matrix calculations with γ = 12.6, 25.1, 62.8 and 88.0. The two groups of PDFs from the RCM and the K matrix calculations agree well with small deviations. This shows that the good connections between the two methods for analyzing the impedance statistics of chaotic systems.
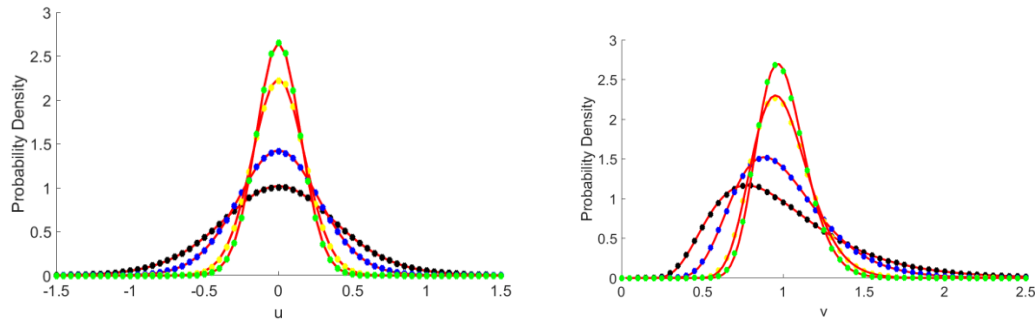
Figure 3.5: PDFs of real and imaginary part of K-matrix from analytical calculations and real and imaginary part of $\underline{\underline{z}}$ matrix from numerical calculations in GUE cases. The five red curves are PDFs of K-matrix from analytical calculations with γ =12.6, 25.1, 62.8, and 88.0. The dots represent the numerical calculations from the RCM, black ($\alpha = 1$), blue ($\alpha = 2$), yellow ($\alpha = 5$), green ($\alpha = 7$).

The comparisons of the K matrix and $\underline{\underline{z}}$ in the GUE case are also examined. In Fig. 3.5, PDFs of impedance statistics from the RCM of four loss parameters are shown. We test the same set of loss parameters, which are $\alpha = 1$ (black dots), $\alpha = 2$ (blue dots), $\alpha = 5$ (yellow dots) and $\alpha = 7$ (green dots). The four red curves are the PDFs of impedance statistics from K matrix calculations with $\gamma = 12.6$, 25.1, 62.8 and 88.0.

From the comparisons above, we can see that the two theories actually deal with the same statistical quantities with just very small deviations. For the numerical calculations of the Random Coupling Model in the GUE case, I follow the procedures described in the previous PhD dissertation of Zheng *et al*. [19] in our group.

3.3 The Random Coupling Model Impedance Statistics with Different Loss Parameters

When the RCM is applied to analyze the electromagnetic problem of a chaotic system, the impedance statistics from a set of data are assumed to be described by a single value of loss parameter α. As the data from a wide range of frequencies are included in the impedance statistics, the loss parameter is expected to vary. In this section, the question of whether or not a single α value is applied in the RCM to describe the impedance statistics with a certain range of loss parameters is discussed.

Normalized impedance statistics numerically calculated based on the RCM are used to analyze the problem. Each data set is calculated with a single α value and there are 200000 data points.

Data Set	$\sigma^2_{Re[z11]}$	$\sigma^2_{Im[z11]}$	$\sigma^2_{Re[z12]}$	$\sigma^2_{Im[z12]}$
$\alpha = 0.1$	4.09	4.16	1.54	1.59

$\alpha = 1$	0.342	0.338	0.160	0.158
Composite Data Set	2.22	2.25	0.85	0.87

Table 3.1: Variances of normalized impedance of $\alpha = 0.1, 1$ and variances of combined normalized impedance statistics.
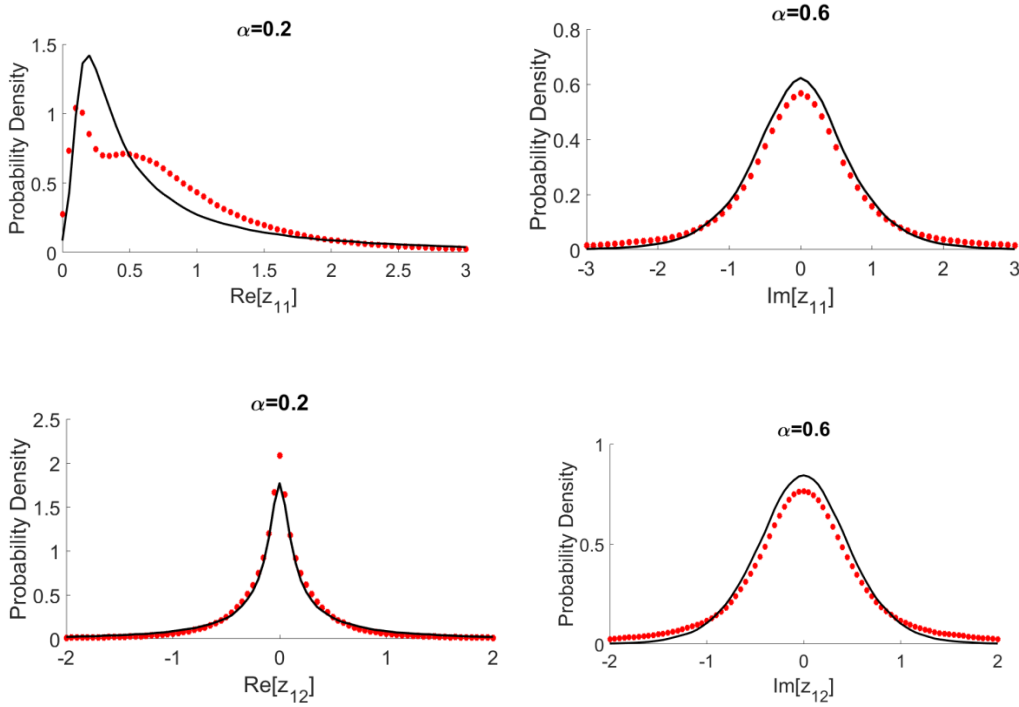
Figure 3.6: PDFs of composite normalized impedance statistics ($\alpha = 0.1, 1$) with the best fitting PDFs from RCM predictions.

We create a composite data set consisting of equal contributions from two data sets with $\alpha = 0.1$ and $\alpha = 1$. In Table 3.1, I have shown the variances for the real and imaginary part of z_{11} and z_{12} for a single value of $\alpha = 0.1, 1$ and the composite data set. In Fig. 3.6, we can see that the PDFs deviate far from the RMT predictions, and no single governing loss

parameter can be determined. Therefore, if the composite data are from systems with very

low and intermediate loss parameter, the new composite data set cannot be described by the

RCM predictions.

Data Set	$\sigma^2_{Re[z11]}$	$\sigma^2_{Im[z11]}$	$\sigma^2_{Re[z12]}$	$\sigma^2_{Im[z12]}$
$\alpha = 1$	0.342	0.338	0.160	0.158
$\alpha = 2$	0.165	0.163	0.080	0.079
Composite Data Set	0.253	0.251	0.120	0.119
$\alpha = 1.5$	0.223	0.221	0.106	0.105

Table 3.2: Variances of normalized impedance of $\alpha = 1, 2$ and variances of combined normalized impedance statistics.
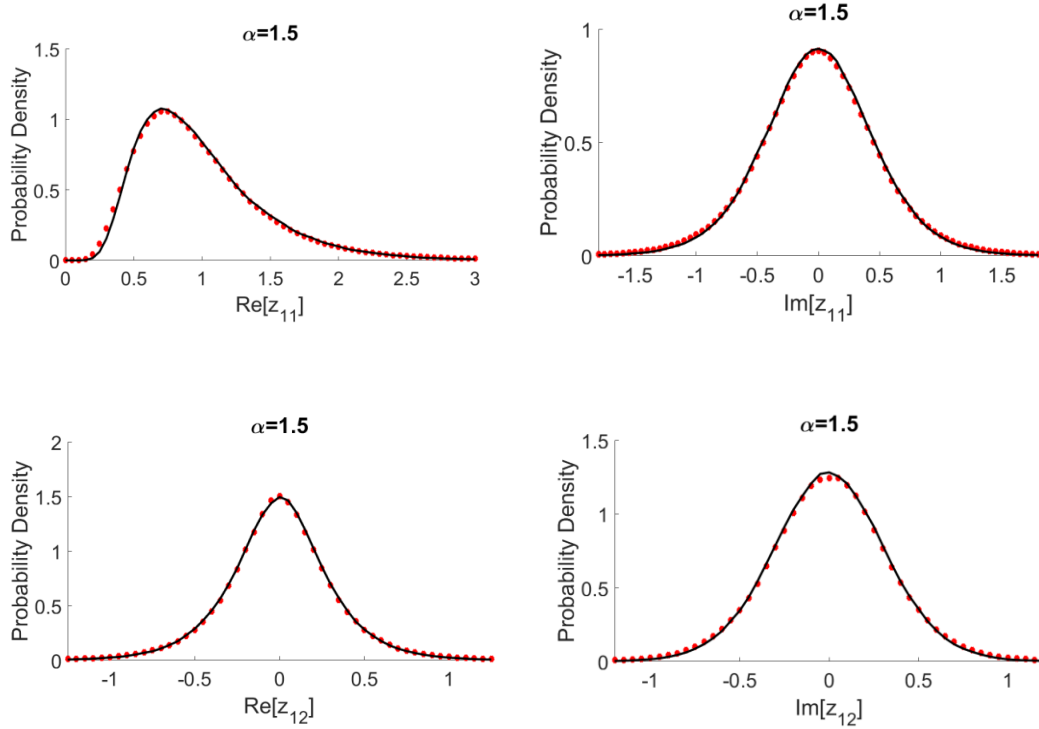
Figure 3.7: PDFs of composite normalized impedance statistics ($\alpha = 1, 2$) with the best fitting PDFs from RCM predictions.

Data Set	$\sigma^2_{Re[z11]}$	$\sigma^2_{Im[z11]}$	$\sigma^2_{Re[z12]}$	$\sigma^2_{Im[z12]}$
$\alpha = 1$	0.342	0.338	0.160	0.158
$\alpha = 1.5$	0.223	0.221	0.106	0.105
$\alpha = 3$	0.108	0.106	0.053	0.052
Composite Data Set	0.224	0.222	0.106	0.105
$\alpha = 1.8$	0.185	0.183	0.089	0.087

Table 3.3: Variances of normalized impedance of $\alpha = 1, 1.5, 3$ and variances of combined normalized impedance statistics.

28
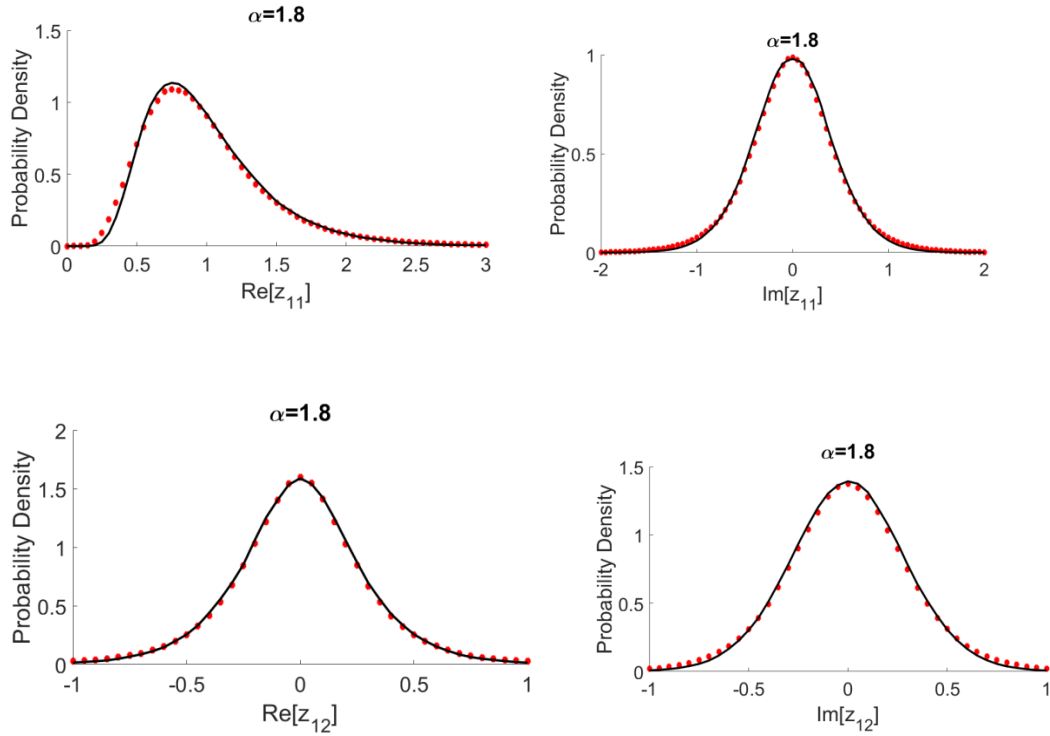
Figure 3.8: PDFs of composite normalized impedance statistics ($\alpha = 1, 1.5, 3$) with the best fitting PDFs from RCM predictions.

In Table 3.2, Table 3.3, Fig. 3.7 and Fig. 3.8, I have tried two different composite data sets, the variances of which are very close. From the plots, we can see that the PDFs of the real and imaginary parts of z_{11} and z_{12} are simultaneously fit (black curves) by RMT with a single loss parameter, $\alpha = 1.5$ and $\alpha = 1.8$. Therefore, we can create composite data set from 2 or more data sets with relatively close loss parameters (with $\alpha > 1$), and the composite data set can be predicted by the RCM well.

Data Set	Estimated α from Im[z11]	Estimated α from Re[z11]
4-6 GHz	1.1	1.4
6-8 GHz	1.8	2

8-10 GHz	2.5	3.1
10-12 GHz	3.5	4

Table 3.4: Estimated α values from the real and imaginary part of z_{11} over different frequency ranges.

α = 1.1; 1.8; 2.5; 3.5
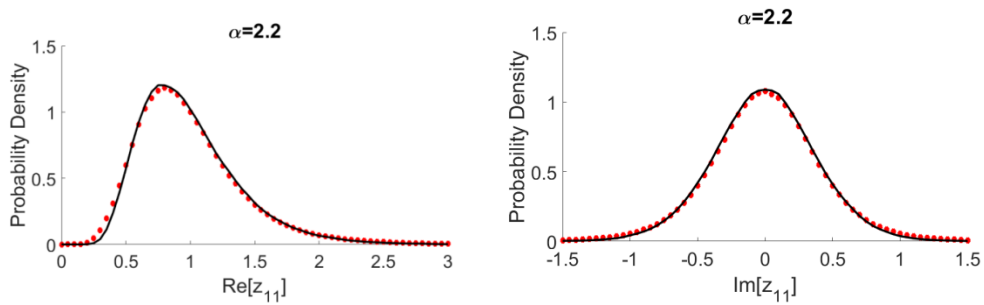
α=1.4; 2; 3.1; 4
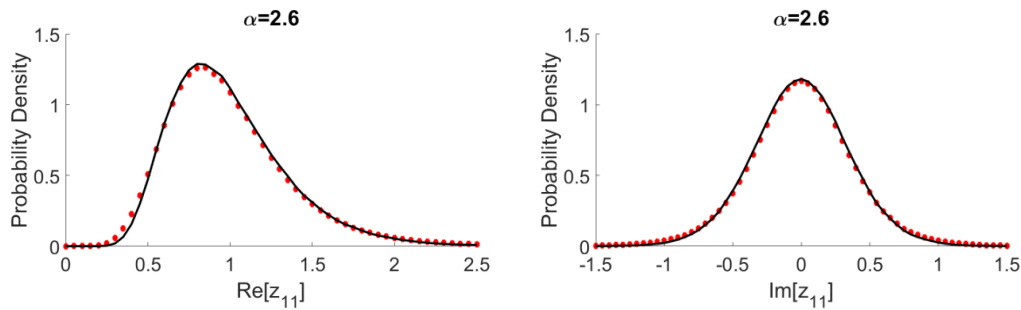
Figure 3.9: PDFs of composite normalized impedance statistics with loss parameters from experimental data from the microwave networks with the best fitting PDFs from RCM predictions.

The last data sets I have tried are created from the loss parameters estimated in experiments with microwave networks which will be introduced in Chapter 4. I want to make sure that we can deal with the statistics from experiment in such ways.

Chapter 4: Experimental Study of Quantum Graphs with Microwave Networks

4.1 One Port and Two-Port Tetrahedral Microwave Networks

4.1.1 Basic Features of Microwave Networks
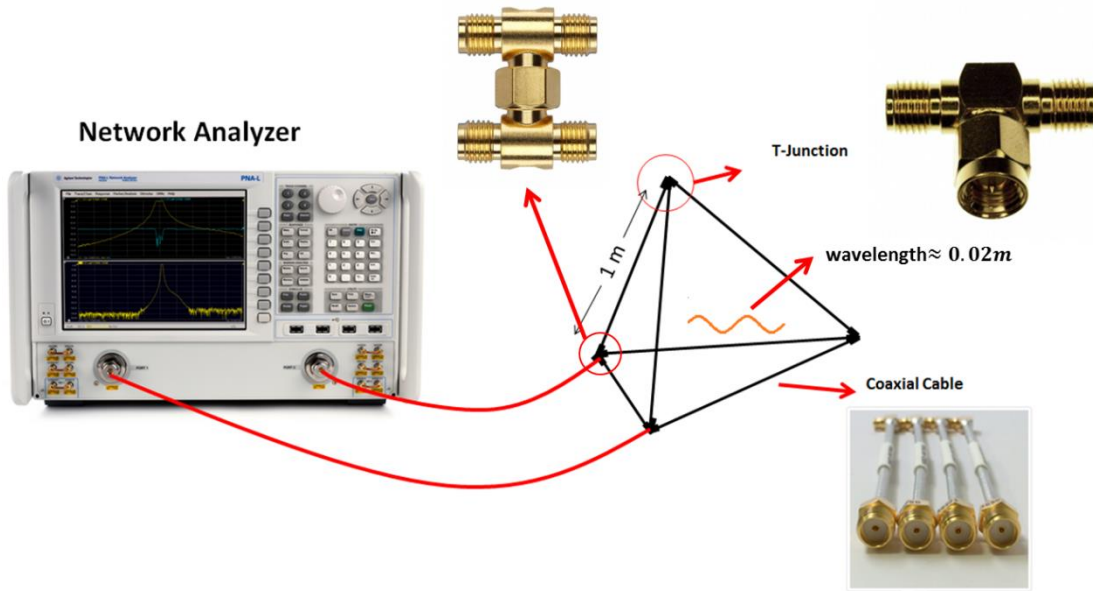
Figure 4.1: Experimental Setup of the microwave networks. The network analyzer (left) is connected to the tetrahedral graph by means of two coaxial cables (shown in red). The ports are made up of two tee-junctions (inset), while the other nodes are simple tee-junctions (upper right inset).

The experimental setup is shown in Fig. 4.1. Coaxial cables are connected by the T junctions to form a tetrahedral network. For the coupling ports, two T junctions are connected to form the 4-coaxial-connector junction. Each cable used in the graph has a unique length. The minimum length of the cables is 1 m and maximum is 1.5 m with the average length of 1.3 m. Hence, the total length of the networks is around 7.8 m. For the frequency range we have measured, the wavelengths range from 0.01 m to 0.05 m, making the graph electrically large and highly over-moded. A network analyzer is connected to two ports of the network

and the 2 by 2 scattering matrix is measured as a function of frequency (or wavenumber) from 1 GHz to 18 GHz.
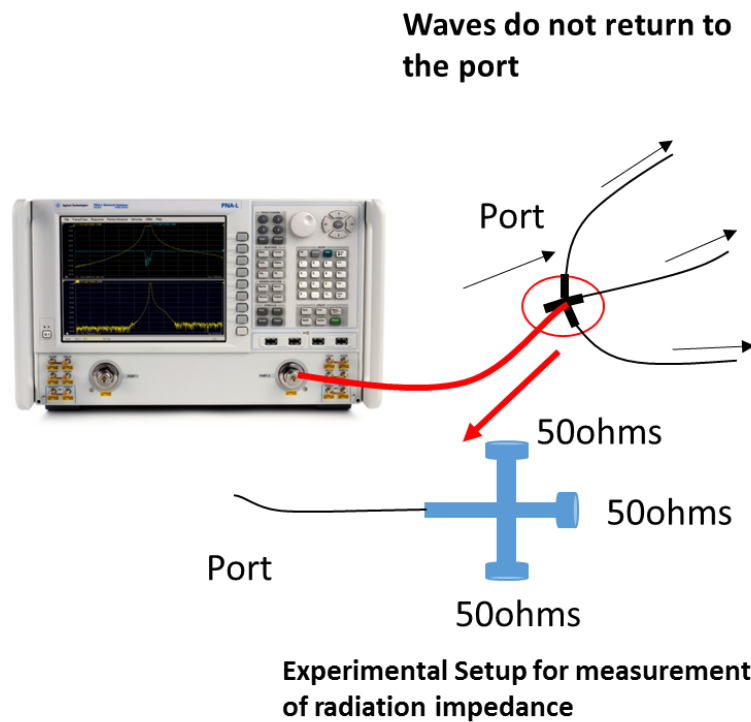
Figure 4.2: Experimental Setup of measuring the radiation impedance of the networks.

One of the properties of the network systems we can measure is the radiation impedance, which is the impedance in the situation that waves go into the system and do not return to the port. In the experiment, to achieve this we can terminate the four-connector coupling port with three 50 Ohm loads as the characteristic impedance of the cable and the T-junctions is 50 Ohms.

The raw data can be examined to yield insights for use in the RCM analysis. Fig. 4.3 shows the resistance and reactance of three kinds of impedance obtained from the measured raw data in the 9 to 10 GHz subset of the data. The blue curve is the impedance of one realization of the network, labeled as Z. The red curve is the impedance averaged over all the

realizations of the graph, labeled as Z_{avg}. The green curve is the measured radiation impedance of the ports, labeled as Z_{rad}. The radiation impedance Z_{rad} was measured by removing the graph in Fig. 4.3 and placing absorptive loads on the three open coaxial connectors of the two ports. From the plots, we can see that Z and Z_{avg} are both fluctuating around the slowly-varying Z_{rad}. The small oscillations in Z_{avg} are manifestations of the short-orbits that survive in many realizations of the networks.
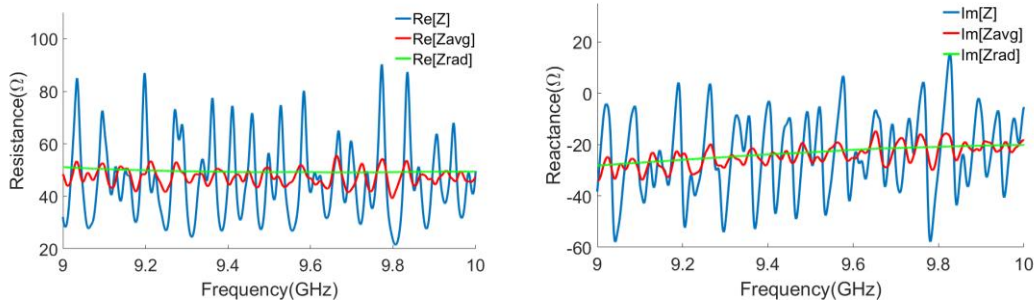
Figure 4.3: Resistance and reactance (real and imaginary parts of impedance) of one realization of a 1-port tetrahedral graph network (blue, labeled Z), averaged impedance over all realizations (red, labeled Z_{avg}), and measured radiation impedance (green, labeled Z_{rad}) from 9 to 10 GHz.

To achieve a randomized electromagnetic environment and a high quality ensemble of the microwave networks, different realizations are generated in the experiment. The system is perturbed globally by changing the total length of the network. In each member of the ensemble one of the bonds is changed to another cable of a different length, and in all about 80 unique realizations are created. To test the quality of this ensemble, the ratio Λ of the maximum transmitted power to the minimum transmitted power at each frequency point for the different realizations is compiled [17].
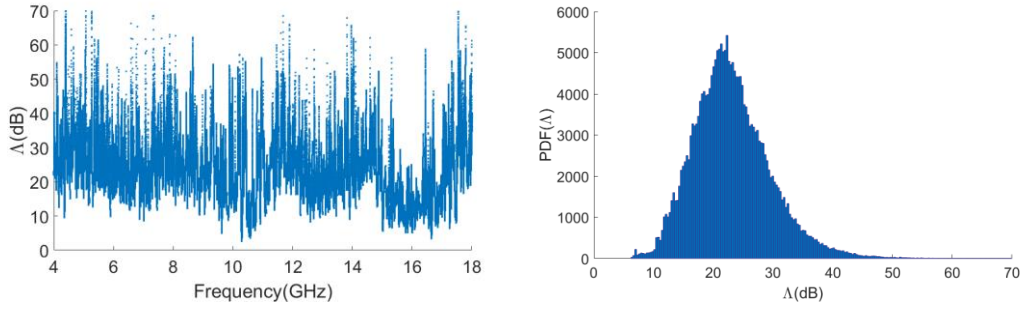
Figure 4.4: Plot of Λ vs. frequency for an ensemble of 81 realizations of the tetrahedral microwave graph. A value of Λ is found for every measured frequency point between 4 and 18 GHz. (b) Histogram of the ratio Λ of the maximum transmitted power to the minimum transmitted power over an ensemble of 81 realizations of the tetrahedral graph.

In Fig. 4.4 we can see that the histogram of Λ is widely spread with a mean of 23 dB and a standard deviation of 6.5 dB. The dynamic range of Λ over the frequency range of 4 to 18 GHz is about 60 dB, and this shows that the ensemble is of high quality and suitable for further statistical analysis [27].
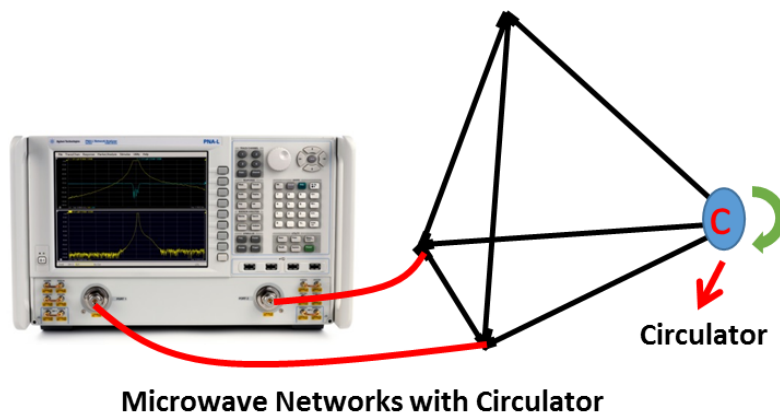
Figure 4.5: Experimental Setup of microwave networks with circulator.

As mentioned in the Introduction, the two symmetries of the chaotic systems are the Gaussian Orthogonal Ensemble (GOE) and Gaussian Unitary Ensemble (GUE). GOE is the system with time reversal invariance and GUE is the system lacking time reversal invariance. For the microwave networks, we try to break the time reversal invariance and analyze the statistical properties of the system in the GUE regime.

The way we break time-reversal invariance is to replace one of the T-junctions with a circulator. By this action we have changed the scattering matrix of the node and change the wave propagations back and forth between the two coupling ports.

Ideally, the scattering matrix of a T-junction is as follows,

$$S = \begin{pmatrix} -1/3 & 2/3 & 2/3 \\ 2/3 & -1/3 & 2/3 \\ 2/3 & 2/3 & -1/3 \end{pmatrix}, \tag{4.1}$$

and the scattering matrix of a circulator is as follows,

$$S = \begin{pmatrix} 0 & 0 & 1 \\ 1 & 0 & 0 \\ 0 & 1 & 0 \end{pmatrix}, \tag{4.2}$$

From the scattering matrix we can see that if a wave goes into the ports of a T-junction, it can 'freely' propagate between the ports. However, if a wave goes into the ports of a circulator, it just propagates in a fixed direction. We can check the raw data of S_{12} and S_{21} of the tetrahedral graph containing the circulator as shown in Fig. 4.6. The two curves are totally different, showing that time-reversal invariance of the graph has been broken.
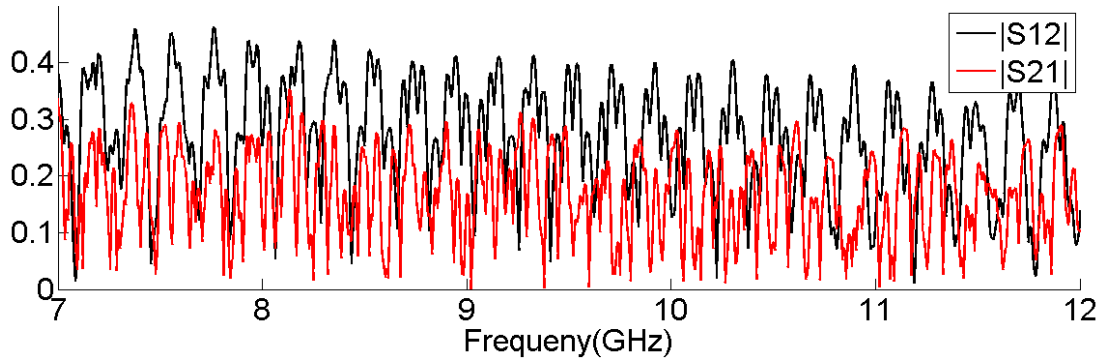
Figure 4.6: The magnitude of S_{12} and S_{21} of the networks with circulator (shown in Fig. 4.5) over the frequency range 7-12 GHz.

Another more efficient and quantitative way to check the degree of time reversal invariance breaking is to calculate the time-reversal asymmetry parameter A

$$A = \int \left(||S12| - |S21|| \right) df / \int \left(|S12| + |S21| \right) df, \qquad (4.3)$$

where the integrals are carried out over one resonant peak.

The parameter A is shown in Fig. 4.7 over a 1 GHz range. Apparently, the parameter A is nearly zero in the case that the networks have no circulator. And the parameter A is fluctuating between 0.1 to 0.7 in this frequency range, when the networks contain a circulator.
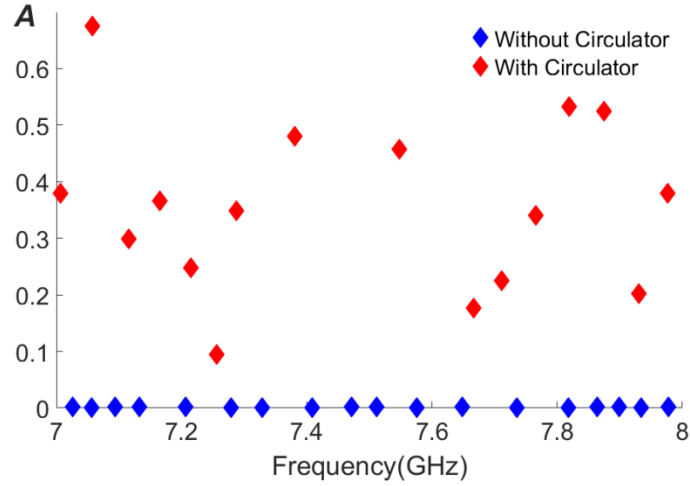
Figure 4.7: Time-reversal asymmetry parameter A over the frequency range 7-8 GHz for both tetrahedral networks without circulator (Blue dots) and tetrahedral networks with circulator (Red dots).

In Hemmady *et al*. [34], for the loss parameter $\alpha \gg 1$, there are some relationships between the variance of the normalized impedance and the loss parameter as follows.

In the case with time reversal invariance (GOE),

$$\sigma^2_{Re[z]} \approx \sigma^2_{Im[z]} \cong \frac{1}{\pi\alpha}, \tag{4.4}$$

and in the case without time reversal invariance (GUE),

$$\sigma^2_{Re[z]} \approx \sigma^2_{Im[z]} \cong \frac{1}{2\pi\alpha}, \tag{4.5}$$

So, there is a factor of 2 difference for the variance between the two cases. We can check this over a frequency range as shown in Fig. 4.8. The variances are obtained for every 2 GHz range from the normalized impedance. From the results we can see that the variances are almost following the equations above.
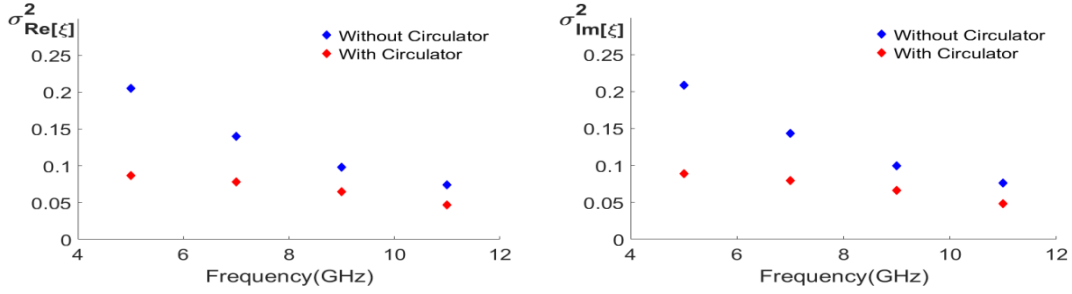
Figure 4.8: Variances of real and imaginary part of normalized impedance of the 1-port microwave networks with and without circulator.

4.1.2 Impedance Statistics of Microwave Networks

As described in Chapter 2, the measured scattering matrix ensemble data can be used to examine the statistics of the normalized impedance matrix $\underline{z}$ in Eq. (2.7) and compared to the predictions of RMT in Eq. (2.2). The matrix $< \underline{\underline{Z}}_{cav} >$ is computed by taking the average of the measured Z_{cav} over all the realizations at each frequency point. The impedance matrix $\underline{\underline{z}}$ is obtained by solving Eq. (2.7) using the measured matrix $\underline{\underline{Z}}_{cav}$ along with $< \underline{\underline{Z}}_{cav} >$. As shown in Fig. 4.3, the averaged impedance $< \underline{\underline{Z}}_{cav} >$ includes the radiation impedance along with the short-orbits effects in the network. The normalization process is expected to remove the non-universal coupling of the ports and the short-orbit effects in the networks, and based on the RCM, the normalized impedance matrix $\underline{z}$ is expected to display universal statistical properties.

First, we check the impedance statistics for one port networks. Since, there is just one coupling port to measure the scattering matrices, we can only obtain the z_{11} statistics. In Fig. 4.9, we show the impedance statistics of the networks without circulator from the data of 4-12 GHz and compare to the RCM predictions in the GOE case. Although there are some deviations from the RCM predictions, the fitting result is pretty good.
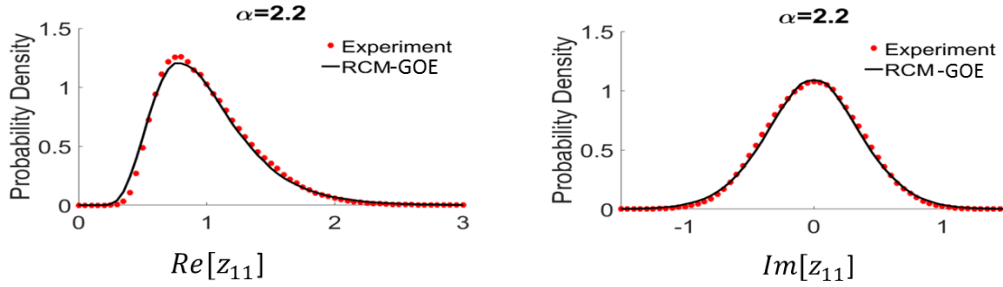
Figure 4.9: Normalized impedance (4-12 GHz) from a 1-Port Graph without Circulator and RCM Predictions (GOE).

In Fig. 4.10, we show the impedance statistics of the networks with circulator from the data of 4-12 GHz and compare to the RCM predictions in the GUE case. We can also get very good fitting results.
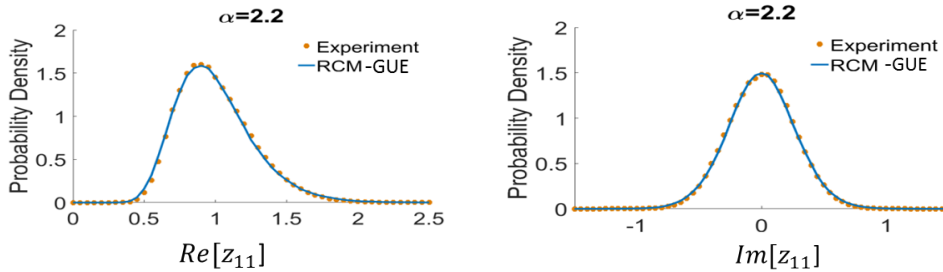
Figure 4.10: Normalized Impedance (4-12 GHz) from 1-Port Graph with Circulator and RCM Predictions (GUE).

In Fig. 4.11, we put the curves of the two cases in the same plot. It is clear that the two curves follow different RCM predictions. And the good thing here is that we get the same loss parameter value in both cases.

I have also tried to fit the curve from networks with a circulator with the RCM predictions in the GOE case. I can get a very good fit, but with a much higher loss parameter.

To make sure that the loss parameter in the two cases are truly the same. I have calculated the quality factor Q for both cases utilizing the time-domain method. And for both cases the quality factor Q is around 390. So the results from the fitting curves are trustable.
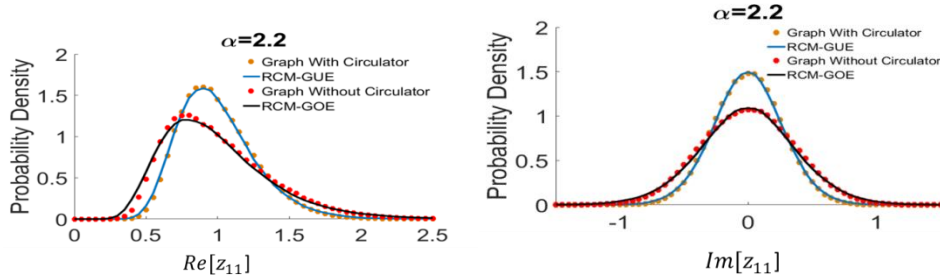
Figure 4.11: Normalized Impedance (4-12 GHz) from One Port Graph both with and without Circulator and RCM Predictions (GOE and GUE).

4.2 Non-universal Features in the Networks

4.2.1 Non-universal Behavior in Impedance Statistics

In the previous section, we have examined the impedance statistics for one-port networks. Next we can examine the two port networks. We can examine the statistics of diagonal and off-diagonal impedance $\underline{\underline{z}}$ elements, as shown in Fig. 4.12, over a large frequency range of 4 to 12 GHz. Over this range the loss parameter of the graphs is expected to vary in a smooth and monotonic manner. In Section 3.3 above, an investigation by means of RCM numerical calculations shows that it is reasonable that the RCM can describe the impedance statistics of data resulting from a composite of different loss parameters.

First we note that all of the PDFs in Fig. 4.12 can be fit to the PDFs predicted by RMT as long as the loss parameter is allowed to vary. In particular, note that the same loss

parameter can be used to fit both the real and imaginary data for a given impedance matrix element (namely z_{11}, z_{12} and z_{21}). It is expected that all impedance matrix elements should have statistics governed by a single value of the loss parameter. However, we note that different loss parameters are required to fit the impedance statistics of diagonal (z_{11}) and off-diagonal (z_{12}, z_{21}) elements. In Fig. 4.12, the PDFs of z_{11} are best fit to RMT with a loss parameter $\alpha = 2.7$, while the PDFs of z_{12} and z_{21} are best fit to RMT with $\alpha = 0.8$. Note that, the loss parameters fitting the two off-diagonal elements (z_{12} and z_{21}) are the same for both real and imaginary parts.

In [18], the RCM was successfully applied to describe the electromagnetic statistics in complex three-dimensional enclosures. However, non-universal behavior similar to that observed here has also been seen in a 3D cavity case [28], where the enclosures have one wall with an electrically-large aperture. In that case any ray inside the cavity that reaches the aperture will exit the system, leading to a source of loss that is not homogeneous. This also leads to the situation that the Berry random plane-wave hypothesis may not be obeyed for waves at the ports.
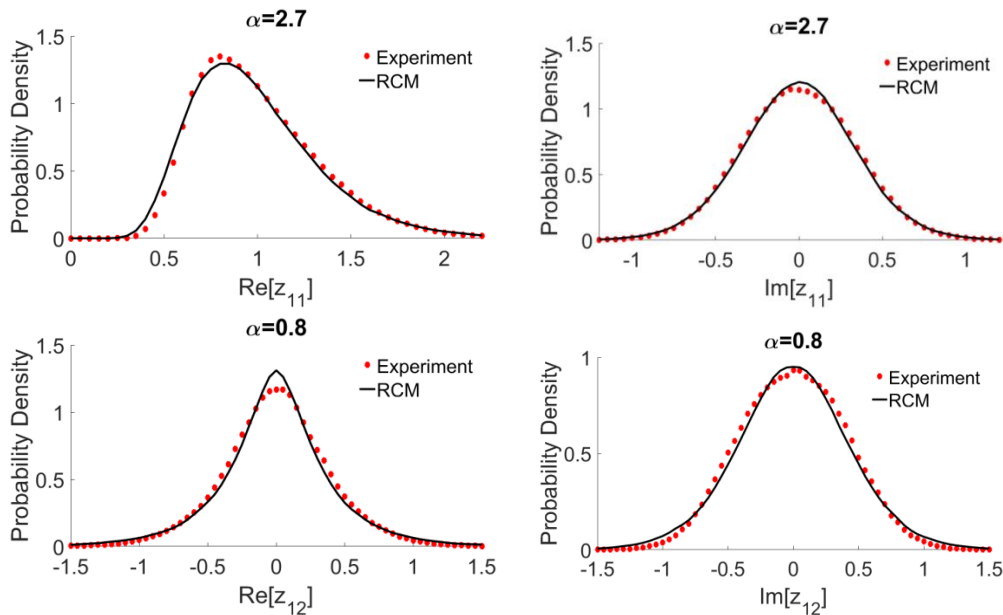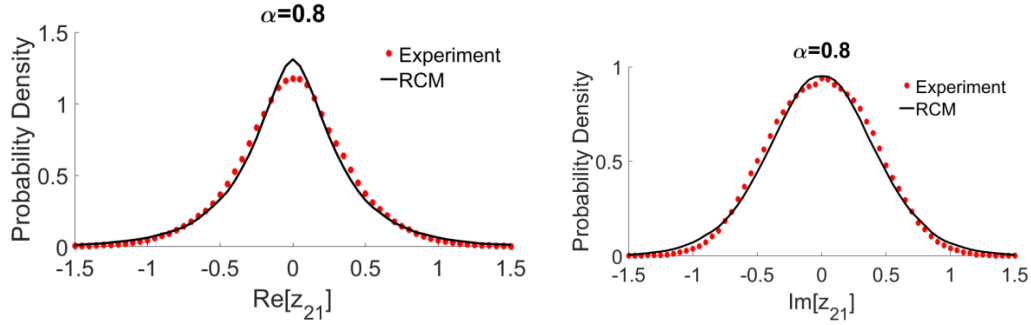
Figure 4.12: PDFs of the real and imaginary parts of z_{11} and z_{12} from experimental measurements of tetrahedral graphs (red dots) and best fit RCM predictions (black curves) with associated α values. The data are from measurements over a frequency range from 4 to 12 GHz.

4.2.2 Numerical Calculation and Quality Factor Calculation

A numerical simulation model of the tetrahedral network is also set up in the Computer Simulation Technology (CST) software as shown in Fig. 4.13. Following the same procedure as in the experimental measurements, the 2 by 2 scattering matrix as a function of frequency can be obtained from the numerical calculation. In this model, the two main modules are the coaxial cable and T-junction. For the coaxial cable block, the parameters for the resistance, dielectric constant, inner and outer diameter of the coaxial cable model are all adjusted to make the S-parameters of the block as close as possible to those of the cables used in the experiment. The lengths of the coaxial cables can be easily changed during the simulation, which allows us to efficiently generate an ensemble of the networks. A Touchtone file with directly measured S-parameter data as a function of frequency is imported as the block for the T-junction (labeled "TS" in Fig. 4.13).
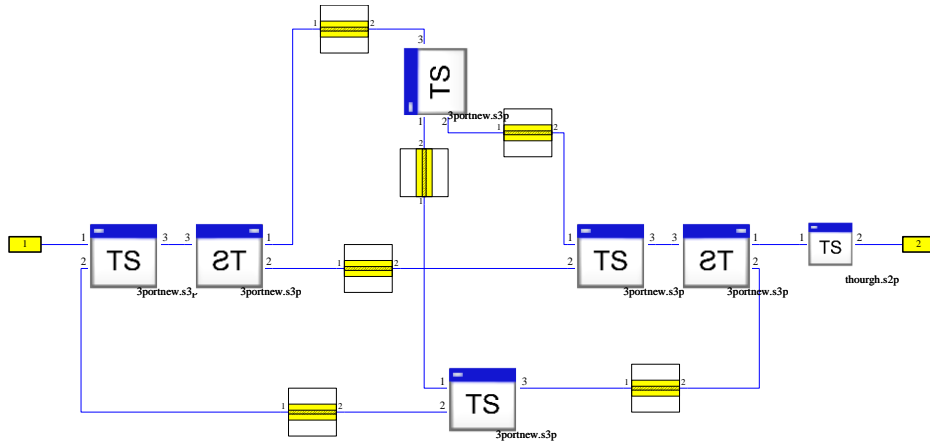
Figure 4.13: Numerical model of the microwave networks in CST. The white and blue blocks represent the scattering matrix as a function of frequency of the T-junctions, and the white and yellow blocks contain the propagation properties of the transmission lines, whose length can be modified. The two ports of the graph are shown as yellow rectangles labeled "1" and "2".

To get deeper insight into the data, the numerical simulation results in CST are treated the same way as the data, and the resulting statistical properties of the impedance matrix elements are presented in Fig. 4.14.
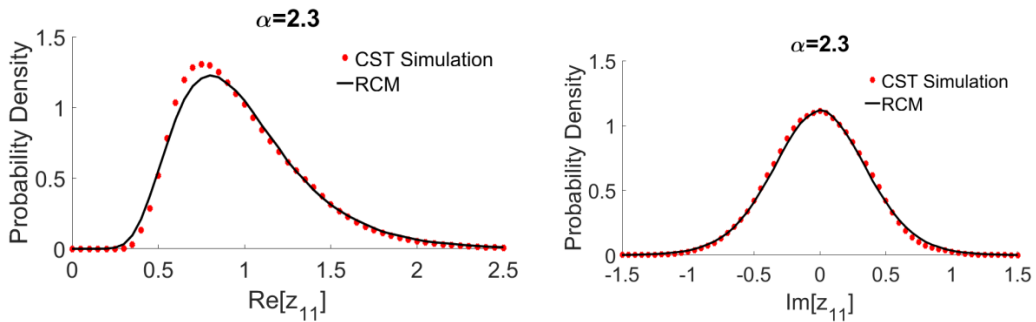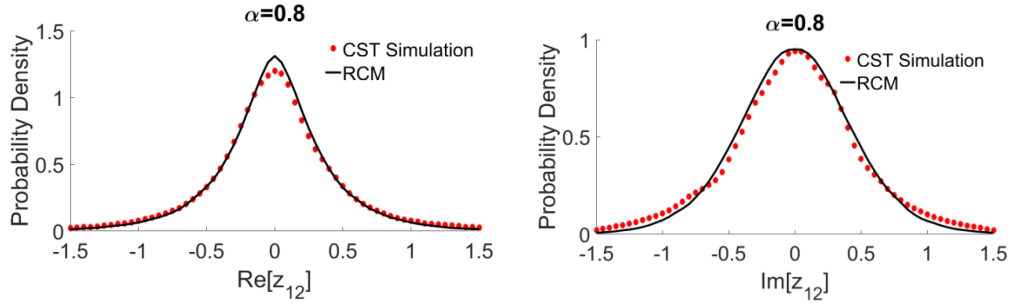
Figure 4.14: PDFs of the real and imaginary parts of z_{11} and z_{12} from numerical simulation of tetrahedral graphs (red dots) and RCM fit predictions (black lines) along with best-fit α values. The data are from calculations in the frequency range from 4 to 12 GHz.

Numerical calculation results show a number of similar features to the data. First there is good agreement with RMT predictions for the PDFs. In addition, the same value for the loss parameter fits both the real and imaginary statistical fluctuations for a given impedance matrix element. However, the same difference in loss parameter fit value between diagonal and off-diagonal impedance matrix elements is seen as in the experimental measurements. In both cases the PDFs of diagonal impedance elements show a higher loss parameter fit value than the off-diagonal impedance elements.

An independent method to check the true loss parameter of the networks is to determine the quality factor Q and, based on Eq. (2.6), evaluate the loss parameter based on the known wavenumber and mean mode spacing of the graph. A time domain method is applied to determine the quality factor Q for a given frequency range, as illustrated in Fig. 4.15.

(a)   (b)
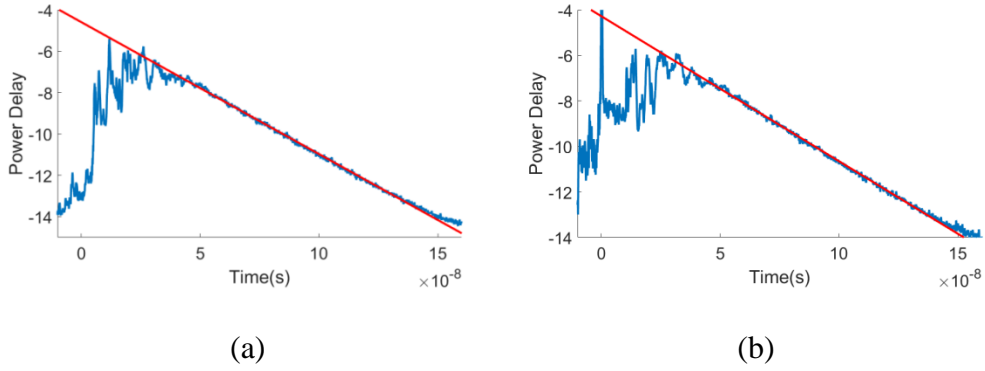
Figure 4.15: Inverse Fourier transform of the measured (a) S_{11} and (b) S_{12} averaged over all realizations to compute the decay time τ for the frequency range 4 to 12 GHz. Both data sets give a clear and consistent single decay time of 7.8 ns, determined from a straight line fit shown in red.

In Fig. 4.15, the inverse Fourier transforms of both measured S_{11} and S_{12}, averaged over all realizations, are plotted in the time domain. The averaged quality factor computed from both spectra is $Q = 394$ for the frequency range from 4 to 12 GHz using the equation $Q = \omega\tau$, where ω is the median value of the frequency range. In Eq. (2.6), k is chosen as the median value for the frequency range, and the loss parameter obtained by this method is $\alpha_Q = 1.1$, which is close to the value fitting the PDFs of the real and imaginary of the off-diagonal impedance matrix elements z_{12} and z_{21} in Fig. 4.12.

One thing we can see that for one-port and two-port cases of the microwave networks, which are generated with the same setup, is that the loss parameters from fitting the PDFs of z_{11} with the RCM predictions are different. In Fig.4.9, the α value is 2.2 for one-port networks and in Fig 4.12 the α value is 2.7 for two-port networks. To verify the deviations, I extract the quality factor of the networks in the two cases.

45

(a)   (b)
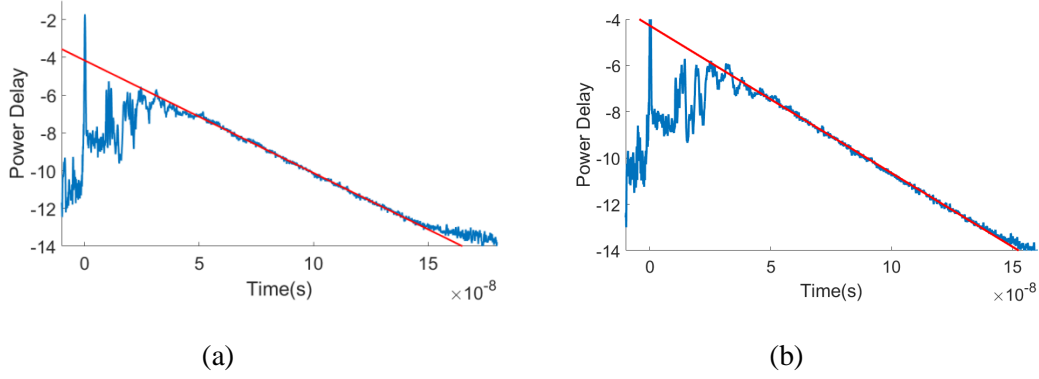
Figure 4.16: Inverse Fourier transform of the measured S_{11} averaged over all realizations to compute the decay time τ for the frequency range 4 to 12 GHz for (a) 1-Port case and (b) 2-Port case. Two data sets give different decay times of 8.4 ns and 7.8 ns, determined from a straight line fit shown in red.

As shown in Fig. 4.16, the decay times computed from the two data sets are different. For the 1-Port case, the decay time is 8.4 ns, so the quality factor $Q = 421$. And the loss parameter α is 1.04, a little bit smaller than the α value from 2-Port case, which is 1.11. I think this is consistent with the method of fitting with PDFs, which may be explained by the fact that the coupling and the reflections from the additional port increases the loss in the system. And this can be observed in the PDFs of normalized impedance which removes the effects of the system-specific features from coupling.

4.2.3 Discussion about the Non-universal Features

Plûhar and Weidenmuller [28] recently showed conditions for universal behavior in quantum graphs and the statistical equivalence to RMT. In [29, 30], experiments with microwave networks are carried out to show the non-universal behavior for long-range fluctuating properties in the spectra of quantum graphs. The universal behavior is obtained only in the limit of infinitely intricate graphs with infinitely many bonds and nodes. In this study, the simple and small tetrahedral networks in the experiment have a finite number of

46

elements, and deviations from universal behavior are expected. Some particularly simple graphs, like the star graph, can show entirely non-universal behavior [32]. In this experimental study, the impedance statistics of tetrahedral graphs show some results similar to the universal behavior but also some deviations from RMT.

The non-universal behavior observed in the data may be due to a breakdown of the random plane-wave (Berry) hypothesis in the graph. This may arise from resonances that occur for waves traveling on the bonds between nodes. Consider a single bond of length L in a much larger graph, and ignore loss. Take b_1 and b_2 to be the amplitudes of the counter-propagating waves at the beginning and end of the bond, and each end of the bond has reflection coefficients ρ_1 and ρ_2 presented by the nodes. The scattered waves from other bonds are considered as sources s_1 and s_2. The two amplitudes can be calculated as,

$$b_1 = \rho_1 b_2 e^{i\phi} + s_1, \tag{4.6}$$

$$b_2 = \rho_2 b_1 e^{i\phi} + s_2, \tag{4.7}$$

where $\phi = kL$ is the phase shift of the wave after it crosses the bond. These equations can be solved for the individual amplitudes as,

$$b_1 = \frac{s_1 + \rho_1 e^{i\phi} s_2}{1 - \rho_1 \rho_2 e^{i2\phi}}, \tag{4.8}$$

$$b_2 = \frac{s_2 + \rho_2 e^{i\phi} s_1}{1 - \rho_1 \rho_2 e^{i2\phi}}, \tag{4.9}$$

Let $R = |\rho_1 \rho_2|$ and $\psi = 2\phi + \arg(\rho_1 \rho_2)$, then a normalized resonance function like that present in the amplitudes given by Eq. (4.10) can be defined as,

$$\lambda^2(\psi) = \frac{1 - R^2}{1 + R^2 - 2R\cos\psi}, \tag{4.10}$$

This function is normalized in the sense that integrating $\lambda^2(\psi)$ over the angles ψ gives unity. Note that the resonance function is bounded by

$$\frac{1-R}{1+R} < \lambda^2(\psi) < \frac{1+R}{1-R},$$ (4.11)

For current conserving, or Neumann boundary conditions at the nodes, we may relate the reflection coefficients to the number of connected bonds, with the coefficients approaching unity as the number of connected bonds increases. Hence the resonance function is unable to be very large or very small when N is a finite number, as in the experiment. Large or small amplitudes for the propagating waves on the bond thus do not show up, but this behavior is not expected in a wave chaotic system. In the case of infinitely large graphs, the resonances (hence amplitudes and impedance values) are expected to be unbounded. This argument suggests that a finite-sized graph, such as that considered experimentally, will not support waves characteristic of a fully wave chaotic system. Hence it is reasonable to expect deviations between the data and RMT statistics such as those observed in this study of simple and small networks. Field-theoretical results for spectral statistics in finite quantum graphs have largely focused on the size of these deviations, and criteria for their disappearance in the limit of large graphs [29, 33].

Prof. Antonsen has proposed that the statistics of the signal level on a bond can be modeled by the following random variable,

$$X_i = \lambda(\psi)\left[N^{-\frac{1}{2}}\sum_{j=1}^{N} Y_j\right],$$ (4.12)

where Y_j are independent, zero mean and unit variance random variables and N is the number of the bonds that are connected to the node of the single bond. A set of random variables characterized by the two parameters N and R. If we assume that N is large then we can expect the sum of the Y's to by a zero mean Gaussian Random Variable. So the variable X has just one distribution depending only on R. If there are no reflections on the node, that means that R is zero and $\lambda = 1$ and it easy to see that X will be a Gaussian Random Variable.
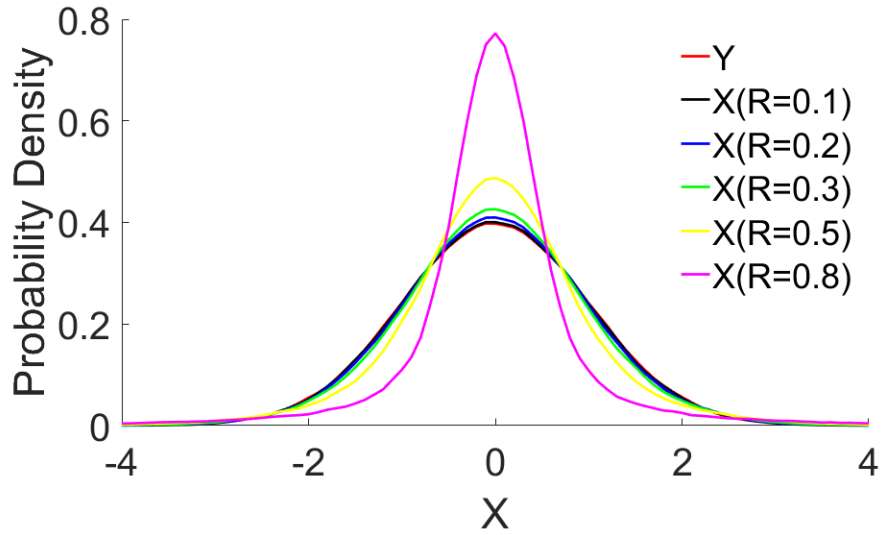
Figure 4.17: PDFs of Y (Gaussian Random Variable) and X with different values of R.

In Fig. 4.17, I have numerically calculated the PDFs of X if Y is a Gaussian Random Variable with different R values when N is a large one. We can see that when R = 0.1 (black curve) that there are just small deviations from PDF of Y (red curve). With the R increasing, the deviations are becoming larger.

(a)

(b)

(c)
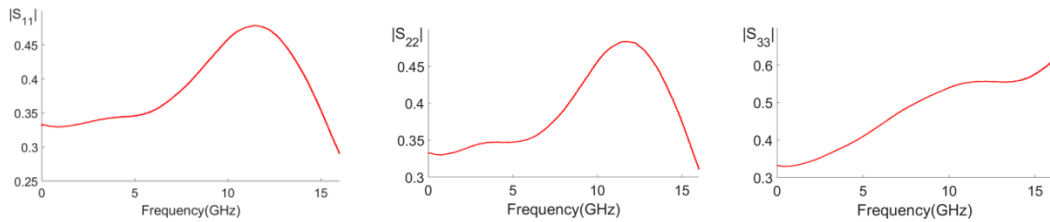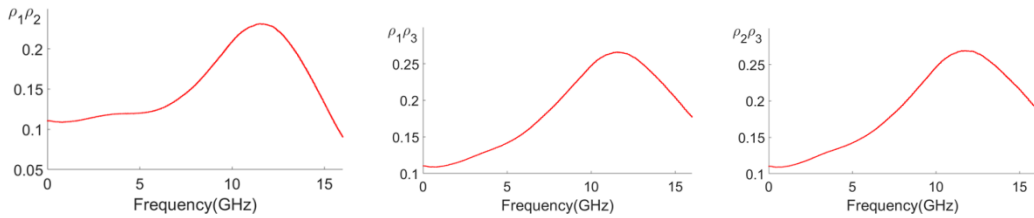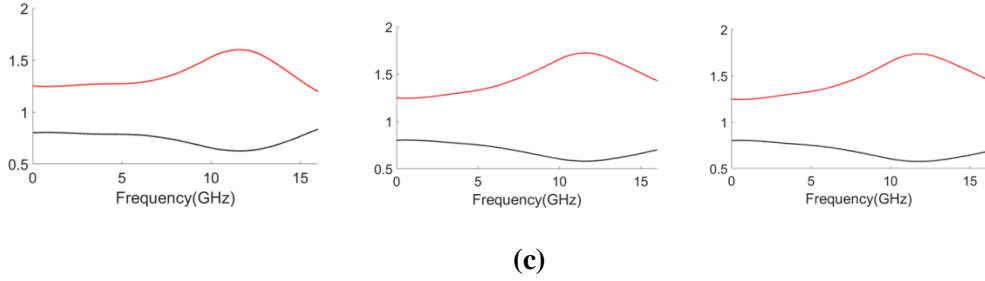
Figure 4.18: Experimental measurements of scattering matrix of T-junctions over the frequency range 0-16 GHz. (a) The magnitudes of reflection coefficients for the three ports on the T-junctions. (b) The calculated R for different combinations of the ports. (c) The values of (1-R)/(1+R) (black curve) and (1+R)/(1-R) (red curve).

I have checked the values of R in the experiment, as shown in Fig. 4.18. In (a), the curves are the raw measured data of the reflection coefficients for the three ports of the T-junctions. The magnitude of the data is very close to the ideal one as shown in the Eq. (4.1), with some deviations over the frequency range. Fig. 4.18(c) shows the range of values of λ, and they varybetween 0.5 and 2.

For the arguments of the non-universal features in the networks, we can check the values of R in Fig. 4.18(b). The Figure shows the values of R range between 0.1 and 0.3. And in Fig. 4.17, we can see that when the R is 0.2 or 0.3, the deviations are clear to see from the Gaussian Random Variable. This suggests that our finite-size tetrahedral graph will not show the universal behavior expected in the limit of very large graph intricacy.

Chapter 5: Conclusions and Suggestions for Future Work

5.1 Conclusions

In this thesis, I have analyzed the electromagnetic coupling problem and wave propagation in complicated systems. For the first-step study, we can focus on studying the quantum graphs realized as microwave networks. In this work, an experimental study of very simple and small quantum graphs simulated by microwave networks is carried out. I have examined some basic features of the microwave networks. This includes the radiation impedance characteristics, and systems with and without time reversal invariance. In addition we have done a lot of work on the impedance statistics analysis. The statistical properties of the impedance matrix of a 2-port tetrahedral graph ensemble displays many properties consistent with random matrix theory. However, a non-universal feature is observed for the impedance statistics. Numerical simulations of similar graphs show very similar non-universal statistical properties. It is argued that because of resonances of the bonds between nodes in the finite-size and small quantum graphs there will be non-universal results.

In addition, I have investigated some other calculations or models related to the Random Coupling Model. For example, the comparison between the RCM and the Power Balance Method, the calculations of the K matrix and the RCM. I hope these new 'little' things can help us in the future studies.

5.2 Future Work

For the future work, the first goal is to further study the non-universal behavior and find a very robust and systematic theory or explanation for it. Right now, we are doing the simulations in the CST microwave studio to show the eigen-modes for a closed microwave network. We are hoping to see that the eigen-modes will have large amplitude at different locations with different quality factor. The expectation is that the eigen-modes have stronger

weight near the coupling ports will have lower quality factor than the eigen-modes with weight around other locations on the networks.

The next step is to set up a process to apply the RCM to numerically calculate the properties of the wave propagations in a complicated system. The aim is to make this model more sophisticated than the existing models based on traditional EM field treatments.

Bibliography

[1] Gabriele Gradoni, Jen-Hao Yeh, Bo Xiao, Thomas M. Antonsen, Steven M. Anlage , Edward Ott," Predicting the statistics of wave transport through chaotic cavities by the random coupling model: A review and recent progress," Wave Motion 51, 606-621 (2014).

[2] Sven Gnutzmann, Uzy Smilansky ," Quantum graphs: Applications to quantum chaos and universal spectral statistics", Advances in Physics, 55, 527-625 (2006).

[3] Oleh Hul, Szymon Bauch, Prot Pakoński, Nazar Savytskyy, Karol Życzkowski, and Leszek Sirko, "Experimental simulation of quantum graphs by microwave networks," Phys Rev E 69 (5), 056205 (2004).

[4] M. Freedman, L. Lovász & A. Schrijver,"Reflection positivity, rank connectivity, and homomorphism of graphs", J. Amer. Math. Soc. 20, 37-51 (2007).

[5] M. Lawniczak, O. Hul, S. Bauch, P. Seba, and L. Sirko, "Experimental and numerical investigation of the reflection coefficient and the distributions of Wigner's reaction matrix for irregular graphs with absorption," Phys Rev E 77 (5), 056210 (2008).

[6] M. Lawniczak, S. Bauch, O. Hul, and L. Sirko, "Experimental investigation of properties of hexagon networks with and without time reversal symmetry," Phys Scripta T135, 014050 (2009).

[7] Michał Ławniczak, Bauch Szymon, Hul Oleh, and Sirko Leszek, "Experimental investigation of the enhancement factor and the cross-correlation function for graphs with and without time-reversal symmetry: the open system case," Phys Scripta T143, 014014 (2011).

[8] F. Haake, *Quantum Signatures of Chaos*, Springer, Berlin, 2 edition, 2000.

[9] H. J. Stockmann, *Quantum Chaos*, Cambridge University Press, Cambridge, England, 1999.

[10] E. P. Wigner, Ann. Math. 53, 36 (1951); 62, 548 (1955); 65, 203 (1957); 67, 325 (1958).

[11] H. Weyl, "Über die Gleichverteilung von Zahlen mod. Eins" Math. Ann. 77, 313 (1916).

[12] S. -H. Chung, A. Gokirmak, D. -H. Wu, J. S. A. Bridgewater, E. Ott, T. M. Antonsen and S. M. Anlage, "Measurement of Wave Chaotic Eigenfunctions in the Time-Reversal Symmetry-Breaking Crossover Regime" Phys. Rev. Lett. 85, 2482 (2000).

[13] T. M. Antonsen, E. Ott, Q. Chen, and R. N. Oerter, Phys. Rev. E 51, 111 (1995).

[14] Isabelle Junqua , Jean-Philippe Parmantier & François Issac, "A Network Formulation of the Power Balance Method for High-Frequency Coupling" Electromagnetics, 25:7-8, 603-622 (2005)

[15] Xing Zheng, Sameer Hemmady, Thomas M. Antonsen Jr., Steven M. Anlage, and Edward Ott, "Characterization of Fluctuations of Impedance and Scattering Matrices in Wave Chaotic Scattering," Phys. Rev. E 73 , 046208 (2006).

[16] J.-H. Yeh, J. Hart, E. Bradshaw, T. M. Antonsen, E. Ott, and S. M. Anlage, "Universal and non-universal properties of wave-chaotic systems," Phys. Rev. E 81, 025201 (2010).

[17] Sameer Hemmady, Xing Zheng, Edward Ott, Thomas M. Antonsen, and Steven M. Anlage, "Universal Impedance Fluctuations in Wave Chaotic Systems," Phys. Rev. Lett. 94, 014102 (2005).

[18] Zachary B. Drikas, Jesus Gil Gil, Hai V. Tran, Sun K. Hong, Tim D. Andreadis, Jen-Hao Yeh, Biniyam T. Taddese and Steven M. Anlage, "Application of the Random Coupling Model to Electromagnetic Statistics in Complex Enclosures," IEEE Trans. Electromag. Compat. 56, 1480-1487 (2014).

[19] X. Zheng, Statistics of impedance and scattering matrices in microwave chaotic cavities: the random coupling model, Ph.D. thesis, University of Maryland, College Park, 2005, http://hdl.handle.net/1903/2920.

[20] J. Hart, Scattering from chaotic cavities: Exploring the random coupling model in the time and frequency domains, Ph.D. thesis, University of Maryland, College Park, 2009, http://hdl.handle.net/1903/9549.

[21] J. A. Hart, T. M. Antonsen, and E. Ott, "The effect of short ray trajectories on the scattering statistics of wave-chaotic systems," Phys. Rev. E 80, 041109 (2009).

[22] H. Schanze, H.-J. StÄockmann, M. Mart¶³nez-Mares, and C. H. Lewenkopf, "Universal transport properties of open microwave cavities with and without time-reversal symmetry," Phys. Rev. E, vol. 71, pp. 016223, 2005.

[23] X. Zheng, T. M. Antonsen, and E. Ott, "Statistics of impedance and scattering matrices in chaotic microwave cavities: Single channel case," Electromagnetics, vol. 26, pp. 3, 2006.

[24] X. Zheng, T. M. Antonsen, and E. Ott, "Statistics of impedance and scattering matrices of chaotic microwave cavities with multiple ports," Electromagnetics, vol. 26, pp. 37, 2006.

[25] R. SchÄafer, T. Gorin, T. H. Seligman, and H.-J. StÄockmann, "Fidelity amplitude of the scattering matrix in microwave cavities," New J. Phys., vol. 7, pp.152, 2005.

[26] Yan V. Fyodorov, Dmitry V. Savin, "Statistics of Impedance, Local Density of States, and Reflection in Quantum Chaotic Systems with Absorption", JETP Letters 80, 725 (2004)

[27] Sameer Hemmady, Thomas M. Antonsen Jr., Edward Ott, Steven M. Anlage, "Statistical Prediction and Measurement of Induced Voltages on Components within Complicated Enclosures: A Wave-Chaotic Approach," IEEE Trans. Electromag. Compat. 54, 758-771 (2012).

[28] J. Gil Gil, Z. B. Drikas, T. D. Andreadis and S. M. Anlage, "Prediction of Induced Voltages on Ports in Complex, Three-Dimensional Enclosures With Apertures, Using the Random Coupling Model," in IEEE Transactions on Electromagnetic Compatibility, vol. 58, no. 5, pp. 1535-1540, Oct. 2016.

[29] Plûhar, H. Weidenmuller," Universal Chaotic Scattering on Quantum Graphs," Phys. Rev. Lett. 110, 034101 (2013).

[30] Barbara Dietz, Vitalii Yunko, Malgorzata Bialous, Szymon Bauch, Michal Lawniczak, Leszek Sirko," Non-universality in the spectral properties of time-reversal invariant microwave networks and quantum graphs," Phys. Rev. E 95, 052202 (2017).

[31] Malgorzata Bialous, Vitalii Yunko, Szymon Bauch, Michal Lawniczak, Barbara Dietz, Leszek Sirko," Power spectrum analysis and missing level statistics of microwave graphs with violated time reversal invariance," Phys. Rev. Lett. 117, 144101 (2016).

[32] Tsampikos Kottos and Uzy Smilansky,"Quantum graphs: a simple model for chaotic scattering,"Journal of Physics A: Mathematical and General 36, 12 (2003).

[33] Gnutzmann and Altland "Spectral correlations of individual quantum graphs," Physical Review E 72, 056215 (2005).

[34] S. Hemmady, A Wave-Chaotic Approach to Predicting and Measuring Electro-magnetic Field Quantities in Complicated Enclosures, Ph.D. thesis, University of Maryland, College Park, 2006, http://hdl.handle.net/1903/3979.

[35] Bisrat D. Addissie, John C. Rodgers, Thomas M.Antonsen, Jr.,"Application of the random coupling model to lossy ports in complex enclosures," 2015 IEEE Metrology for Aerospace(MetroAeroSpace), Benevento, 2015, pp.214-219,DOI: 10.1109/MetroAeroSpace.2015.7180656.

[36] Baum, C. E. 1989. "The theory of the electromagnetic interference control," Interaction Notes, : 478

[37] C. L. Holloway, D. A. Hill, J. M. Ladbury, P. F. Wilson, G. Koepke, and J. Coder,"On the Use of Reverberation Chambers to Simulate a Rician Radio Environment for Testing of Wireless Devices". IEEE Transactions on Antennas and Propagation, 54(11):3167-3177, November 2006.